FLOW SEPARATION BY INTERFACIAL UPWELLING IN THE COASTAL OCEAN

by

Xiaojun Jiang

B.Sc., Ocean University of Qingdao, Qingdao, China, 1992

A Thesis Submitted in Partial Fulfillment of

the Requirements for the Degree of

MASTER OF SCIENCE

in

THE SCHOOL OF EARTH AND OCEAN SCIENCES

We accept this thesis as conforming to the required standard

[redacted]

Dr. C. Garrett, Supervisor (School of Earth and Ocean Sciences)

[redacted]

Dr. I. Fung, Departmental Member (School of Earth and Ocean Sciences)

[redacted]

Dr. A. Weaver, Departmental Member (School of Earth and Ocean Sciences)

[redacted]

Dr. N. Djilali, External Examiner (Department of Mechanical Engineering)

Supervisor: Dr. Chris Garrett

Abstract

Coastline curvature is an important factor that causes coastal currents to separate from the boundary. Laboratory experiments have suggested that the separation of a reduced gravity surface current from a corner occurs when $\rho < u/f$, where ρ is the local radius of curvature, u is the characteristic flow speed, and f is the Coriolis parameter. An inviscid, reduced gravity model, in which the current is insulated from the interior by a density front, is used to explore the hypothesis that the centrifugal upwelling of the density interface is one mechanism of flow separation, and separation criteria are derived for various coastal currents under the assumption that the length scale of the alongstream variations is long compared to the width of the current. Uniform potential vorticity δ is used for simplicity.

Two cases have been studied, one with a vertical sidewall (Klinger 1994), the other a sloping one. Model results for the vertical case agree with Klinger's (1994) computations and also agree reasonably well with laboratory results. Cases with different slopes are compared, with h_0, the upstream depth at the interface intersection point y^*, and W_0, the distance from y^* to the offshore edge, being the same as for the vertical case. The results are almost identical to the corresponding vertical ones when the slope s (multipled by R/h_0) is greater than 2, where R is the internal Rossby radius based on h_0. As s decreases, ρ_c decreases. Also, the current at the separation point speeds up more. When the velocity decrease near the bottom due to friction is taken into consideration, cross-stream flow will result. The flow switches from offshore to inshore when, in non-dimensional form, $\bar{u} > (\rho + y)/2$.

The consistency of the neglect of longshore derivatives is checked just upstream

of the separation point. The ratios between the neglected terms and the maximum of the retained terms are $O(1)$ for the vertical case, indicating that the approximation is not valid there; the ratios in the sloping case decrease with decreasing s and are less than 0.5 when $s < 2$.

[redacted]

Dr. C. Garrett, Supervisor (School of Earth and Ocean Sciences)

[redacted]

Dr. I. Fung, Departmental Member (School of Earth and Ocean Sciences)

[redacted]

Dr. A. Weaver, Departmental Member (School of Earth and Ocean Sciences)

[redacted]

Dr. N. Djilali, External Examiner (Department of Mechanical Engineering)

Table of Contents

List of Figures

Acknowledgements

I consider it a great privilege to have studied with my thesis supervisor, Professor Chris Garrett, whose intuitive insight into the nature of a problem and the ability to formulate it simply in mathematics I have always admired. I am deeply grateful to him – his guidance and high standard, his patience and encouragement, as well as his fiancial support. I also thank his wife Elizabeth for her care and understanding.

I would like to thank committee members Andrew Weaver and Inez Fung for their support. Many thanks go to Elina Tragou, Tertia Hughes and all my other dear fellow students, for their friendship, support and help. Thanks to Warren Lee, Amit Tandon and Rosalie Rutka for their help and friendship.

I thank many wonderful people from Emmanuel Baptist Church for their acceptance, support and prayers. Special thanks go to Mary Dixon, Joan Sedgwick and the Career's group, without whom I could never have come to this stage. I thank Lezhen Cai, Xiwei Wu and Bosco Chang for their support and prayers. I would also like to thank Mary Hampton and Christine Ward for their understanding, love and support while I was living with them.

No words can fully express my gratitude to my dearest family – my Mom, Dad and sister for their unconditional love which means so much to me.

So many people have helped and supported me along the way that I cannot possibly list them all. But I want them to know: I shall always cherish their love and kindness.

To God,

who has been my strength and Counsellor,

and whose love and faithfulness have sustained me till this day.

Chapter 1

Introduction

Sometimes when a coastal current encounters coastline irregularities, it separates from the coast. Examples of major boundary currents separating at coastline irregularities include: the Agulhas Current at the southern terminus of the African continent, the Gulf Stream at Cape Hatteras, the Kuroshio at Cape Inubozaki and the Eastern Australian Current near Sugarloaf Point.

Eddies/gyres are often generated following flow separation. One example occurs in the Barrow Canyon near the northern coast of Alaska (Figure 1.1a). Summertime water from the Pacific Ocean flows northward through Bering Strait, across the Chukchi Sea into the Beaufort Sea and is concentrated into a strong current in the Barrow Canyon. Figure 1.1b reveals a strong downcanyon flow that narrows, intensifies and separates off Point Barrow. This is often associated with sub-mesoscale vortices in the Beaufort Sea (D'Asaro 1988). Another example of flow separation is the Mediterranean Undercurrent which flows as a wall-bounded jet along the continental boundary south of Portugal. A tendency for it to separate from the boundary at Cape St. Vincent has been observed by Ambar and Howe (1979a,b) and Bower et al. (1994).

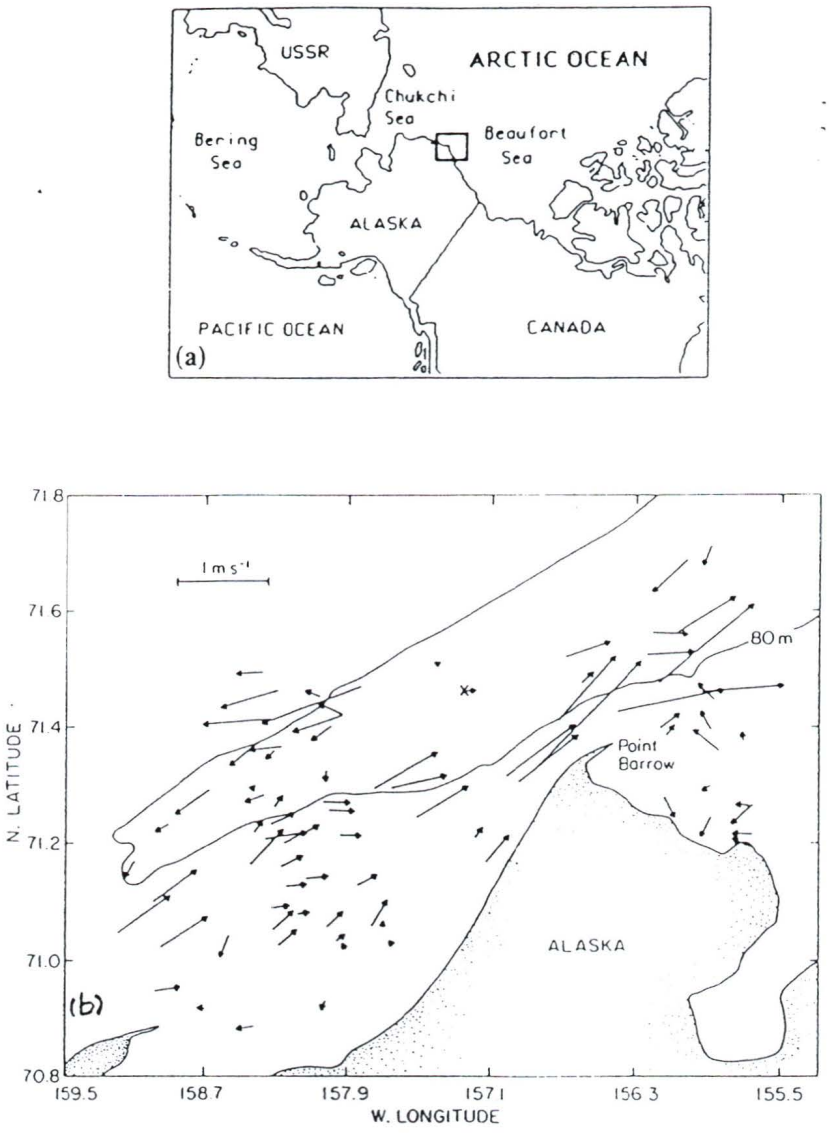

Figure 1.1: (a) Location of Barrow Canyon (from Greenbern et al. 1979 and Garrison et al. 1976). (b) Surface currents measured August 8–16, 1976, using an air-deployed dye-tracking technique (Hufford et al. 1977). Each arrow indicates the measured current at the location given by its center. The 80-m depth contour is indicated.

A situation similar to a coastal boundary current flowing around a corner is the outflow from a strait into a basin, where the outflow may separate at the mouth, and sometimes gyres are formed. Such anticyclones have been observed in the Alboran Sea in the western Mediterranean (Donde Va Group 1984; Lanoix 1974) (Figure 1.2) and in the outflow of the Tsugaru Sea in Japan (Conlon 1982; Kawasaki and Sugimoto 1984). The Alboran gyre is fed by the surface current which flows into the Mediterranean from the Strait of Gibraltar and detaches from a bend in the North African coast. The Tsugaru outflow is also a surface current, which has a seasonal change between a mode that remains attached to the coast and one that forms a gyre.

Separation of tidal currents and generation of eddies behind islands and headlands has been observed in a variety of coastal environments (Pingree 1978; Wolanski et al. 1984; Black and Gay 1987; Pattiaratchi et al. 1987; Geyer and Signell 1990).

Coastline curvature, perhaps not coincidentally, is present in all the examples given above. Thus, it seems to play an important role in flow separation. Though intuitively, one would not expect a swift current to go around a sharp corner, the precise physical mechanism needs to be addressed.

Previously, two main kinds of mechanisms of flow separation due to coastline curvature have been proposed, namely, boundary layer separation for viscous, homogeneous flow and interfacial-upwelling separation for inviscid, two-layer flow (Klinger 1994). These are reviewed in the Chapter 2. In Chapter 3, I describe in some detail Klinger's work on interfacial-upwelling separation where the coast has a vertical sidewall (vertical case). I then extend Klinger's work to include a more realistic sloping sidewall (sloping case) in Chapter 4. The consistency of the assumption in both interfacial-upwelling models is checked in Chapter 5. Applications of the results, discussion and conclusions are given in the last chapter.

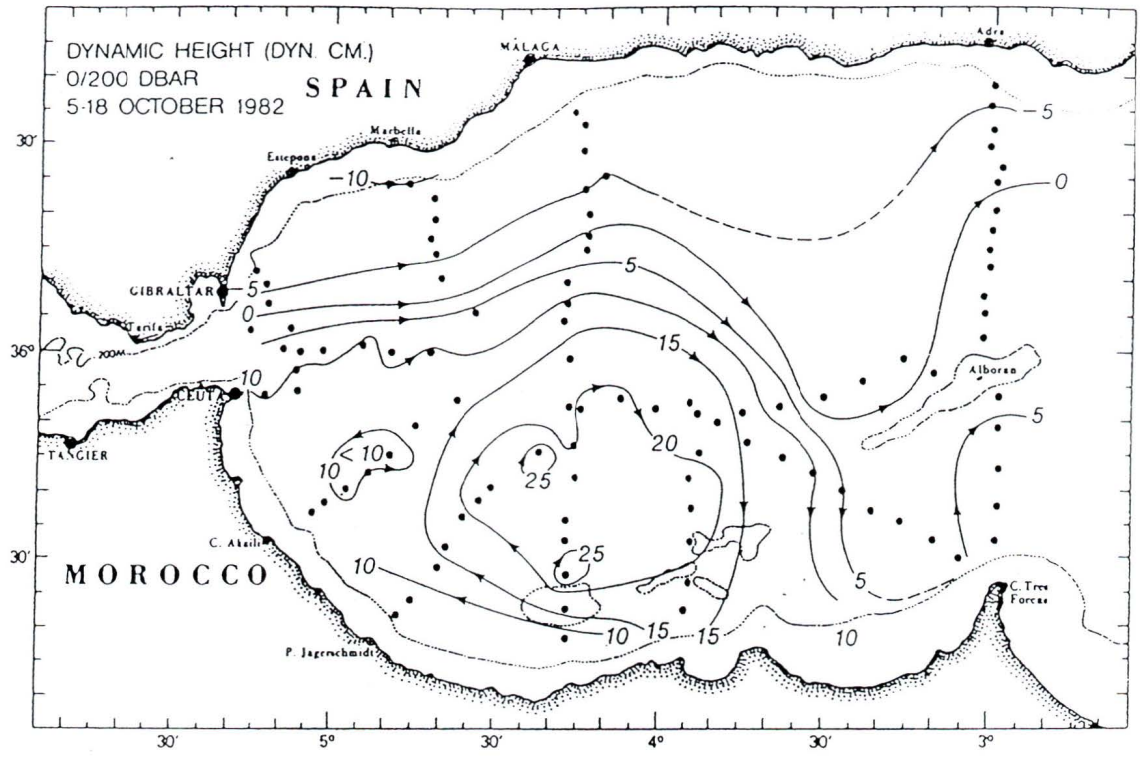

Figure 1.2: The Alboran gyre as seen in a dynamic height map (after Donde Va Groupe 1984).

Chapter 2

Previous Work

Two main kinds of mechanisms have been proposed to explain the separation of a coastal current from a curved coastline. One is boundary layer separation in a viscous, homogeneous model, the other is interfacial-upwelling separation in an inviscid, reduced gravity model.

2.1 Boundary Layer Separation

In reviewing the much observed phenomenon of flow separation and consequent eddy formation behind headlands in some coastal waters, Signell and Geyer (1991) discussed the mechanism of boundary layer separation.

In their model, the bottom is flat except for a shoaling region near the coast in which the depth decreases linearly to H_0 at the boundary. The bottom friction is linearized. Thus, in the interior, there is no mechanism of vorticity generation. Vorticity is generated only in the boundary layer through the torque of the bottom friction in warter of variable depth. Thus, they are able to treat the flow as an irrotational interior plus a thin boundary layer and greatly simplify the dynamics by using the boundary layer approximation (Batchelor 1967; Schlichting 1979). A

schematic is shown in Figure 2.1, where the curved surface represents the headlands or other convex coastlines.

Outside the boundary layer, the flow accelerates upstream of the corner and decelerates downstream because of the convergence and divergence of the streamlines. This causes the pressure to fall upstream and to rise downstream according to the Bernoulli effect. Thus the flow maximum and the pressure minimum coincide. Inside the boundary layer, according to boundary layer theory, the pressure is approximately uniform across the layer, so the pressure gradient close to the solid surface is equal to that at the edge of the boundary layer, which can be found from the solution of the irrotational outer flow. Therefore, inside the boundary layer, the pressure gradient is favourable upstream of the corner and adverse downstream with a zero at the corner. The favourable pressure gradient keeps the flow moving downstream while the adverse pressure gradient extracts momentum from the flow and slows it down. Unless there is enough viscous flux of momentum from the interior, the flow in the boundary layer will turn back at some point. The point along the boundary where the stress $\partial u/\partial y$ vanishes is called the point of *separation.*

For viscous fluid without bottom friction, the advective terms are small near the solid boundary. Thus the momentum balance is between the pressure gradient and the horizontal stress divergence

$$\frac{\partial p}{\partial x} = \nu \frac{\partial^2 u}{\partial y^2}, \tag{2.1}$$

where x and y are the alongstream and cross-stream coordinates, respectively, u is the alongstream velocity, ν is the horizontal eddy viscosity, and p is the pressure. An adverse pressure gradient does not result in immediate flow reversal and separation; it only requires that near the boundary the alongstream velocity profile has an inflection point. Physically, this means that the flow will not separate as long as

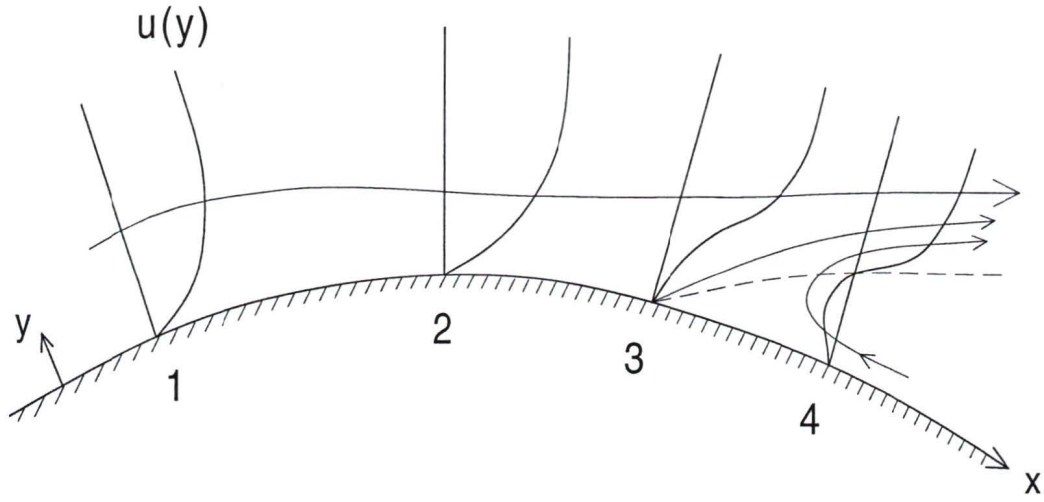

Figure 2.1: Velocity profiles across boundary layer on a curved surface. The pressure gradient changes from being favourable upstream from point 2 to being adverse downstream from it. Point 3 is the separation point. The dashed line separates the forward and backward flows. At point 4, flow reverses due to the strong adverse pressure gradient (after Kundu 1990).

the cross-stream momentum flux is strong enough to balance the deceleration due to the adverse pressure gradient. In most boundary layers, only a small adverse pressure gradient can be supported, and flow separation typically occurs soon after the pressure gradient reverses. The distance between the point of minimum pressure and the point of separation depends on the momentum flux from the interior into the boundary layer as well as the strength of the adverse pressure gradient.

In the coastal ocean, however, the water depth is shallow compared to the horizontal scale of current variation, and bottom friction is often important. This changes the relationship between the irrotational velocity field and the pressure gradient in that the pressure minimum no longer coincides with the velocity maximum. Rather, the point of the minimum pressure occurs downstream of the point of maximum velocity because the pressure gradient has to balance the bottom drag as well as advection.

Bottom friction also changes the relationship between the pressure gradient and the point of flow separation by altering the way momentum is extracted from the boundary layer. This can be shown by a simple analysis of the boundary layer equation very close to the boundary. As the depth goes to zero at the coast, the advective terms are again negligible. If the viscous terms are also negligible, the balance now is between the pressure gradient and the bottom drag

$$\frac{\partial p}{\partial x} = -\frac{C_D u|u|}{h}, \tag{2.2}$$

where C_D is the drag coefficient and h is the water depth. In the absence of transverse viscous stresses, there is no momentum flux from the interior to accelerate the flow, so flow separation occurs as soon as an adverse pressure gradient is established (Signell and Geyer 1991).

2.2 Interfacial-Upwelling Separation

Røed (1980) and Ou and de Ruijter (1986) addressed the effect of coastline curvature on the separation of rotating, stratified flow. They used an inviscid, reduced gravity model with the bottom layer being motionless. Upstream of the region of curvature, the upper layer thickness and velocity are related by geostrophy, but near the corner, centrifugal terms, which are associated with the turning of the current, become important and hence alter the velocity and thickness profiles across the current. The authors found that increasing the curvature of the wall, as one travels downstream from a region of zero curvature, decreases the layer thickness at the wall. At some critical radius of curvature, the thickness becomes zero, which indicates that if a rounded corner has a curvature greater than the critical one, separation from the coast will occur.

To model the surface outflow of the Atlantic water from the Strait of Gibraltar into the Alboran Sea and the possible gyre formation there, Whitehead and Miller (1979) and Bormans and Garrett (1989) did some laboratory experiments on a rotating turntable, with a two-layer current flowing through a channel into a wider basin. Whitehead and Miller concluded that the critical radius of curvature at the corner is the Rossby radius of deformation, whereas Bormans and Garrett concluded that it should be the inertial radius of the current u/f (u is the current speed and f is the Coriolis parameter) instead. Bormans and Garrett (1989) also proposed that their separation criterion was due to a balance between the Coriolis force tending to hold the current to the coast and the centrifugal forces allowing separation to occur.

Inspired by the above work, Klinger (1994) used the inviscid, reduced gravity model of Røed (1980) and Ou and de Ruijter (1986) and derived the separation criteria for coastal currents with uniform potential vorticity. He found that separation

occurs when centrifugal forces at the corner raise the density interface to surface. For a current bounded on the offshore edge by a density front, the critical radius is approximately that found in the laboratory by Bormans and Garrett (1989).

Chapter 3

Interfacial-Upwelling Separation (Vertical Case)

Klinger (1994) has determined the critical radius of curvature for a coastal current to separate when the coastal sidewall is vertical. Here, I would like to review his work, though the arrangement is very different from Klinger's, with many explanations and physical interpretations of my own added. Then, in the next chapter, my work on the case with a sloping sidewall will be presented. We can then compare the two cases to see if the slope of the wall makes any difference.

3.1 Governing Equations

Let us consider a two-layer model which is shown schematically in Figure 3.1. The fluid has two layers, with the bottom layer being motionless. The densities are σ and $\sigma + \Delta\sigma$, respectively. Confined to the upper layer and insulated from the interior by a density front, a boundary current is flowing with the coast on its right. The upstream point is chosen where the coastline is straight ($\rho = \infty$). As one travels downstream, the coastline starts to have some curvature, with ρ, the local radius of

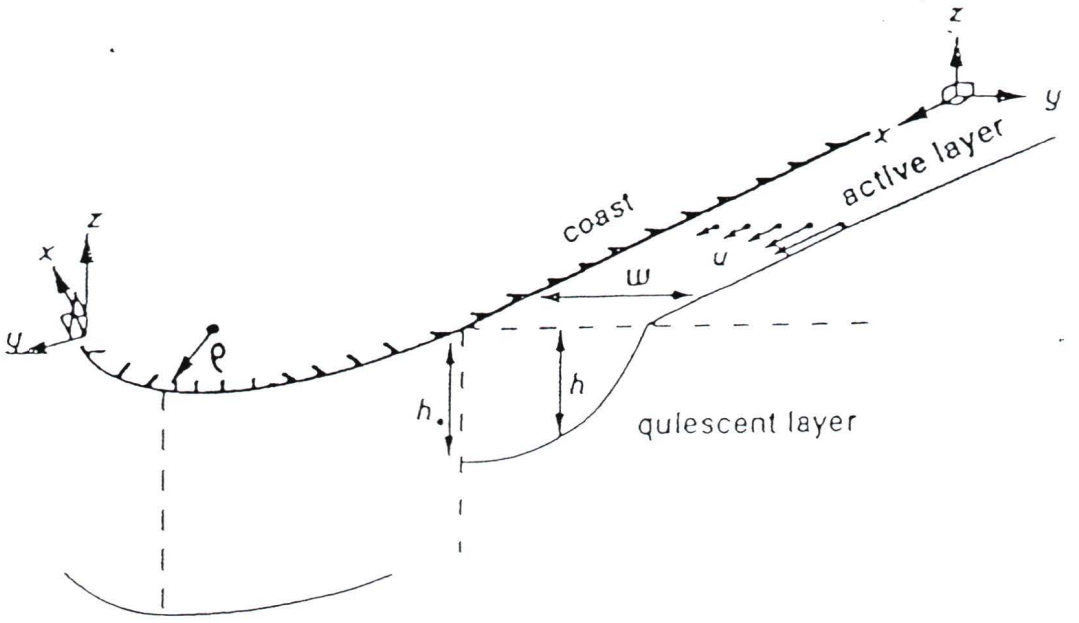

Figure 3.1: The curvilinear coordinates and upstream current structure in a reduced gravity model, where x and y are alongshore and off-shore coordinates, respectively. The current, flowing with the coast on its right, is confined to the upper layer and insulated from the interior by a density front. ρ is the local radius of curvature of the coastline. The upstream point is chosen where the coastline is straight ($\rho = \infty$), and the downstream point usually refers to where ρ is finite. The sidewall at $y = 0$ is vertical (from Klinger 1994).

curvature, being finite. In this thesis, this is usually referred to as the downstream point. The interface tilts up at the wall as the curvature increases, and, at some critical curvature, the interface outcrops at the wall and separation occurs. The main objective of this model is to determine the critical radius of the curvature of the coast, beyond which the current will separate.

Figure 3.2 shows the diagram of the cross-sections of the system at the upstream point where the coastline is straight and at the downstream point where the coastline has some curvature.

Following Røed (1980), we use the curvilinear coordinates as shown in Figure 3.1, where x, y are the coordinates parallel and perpendicular to the shore, respectively. If the fluid under study is Boussinesq, hydrostatic, inviscid and in steady state, then by assuming that the alongshore variations occur on a scale large compared to that of the cross-shore one, we get the simplified cross-shore momentum equation (see the Appendix):

$$fu - \frac{u^2}{\rho + y} = -g' h_y, \tag{3.1}$$

where u is the alongshore component of velocity, h is the upper layer thickness and ρ, the local radius of curvature of the coastline, is a function of the alongshore coordinate x. The sign convention is that a convex (concave) coastline has a positive (negative) ρ, f is the Coriolis parameter, g' (defined by $g(\Delta\sigma/\sigma)$) is the reduced gravity. Equation (3.1) states the geostrophic balance between the Coriolis force and the pressure gradient, with an additional centrifugal term $-u^2/(\rho + y)$ due to the presence of the coastline curvature.

For an inviscid fluid, potential vorticity is conserved along the streamlines and hence is equal to its upstream value. For simplicity, the upstream potential vorticity is assumed constant with a positive value of δ. Thus the conservation law gives the

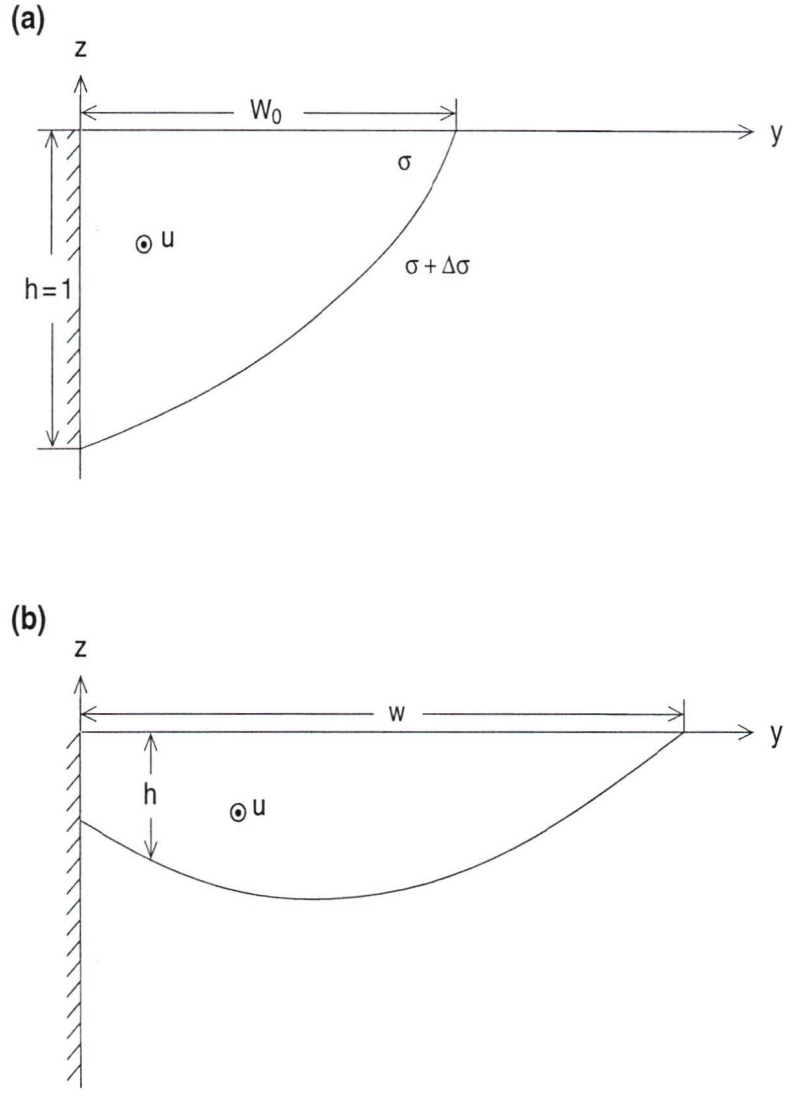

Figure 3.2: Cross-sections of the current in a reduced gravity model (a) upstream with $\rho = \infty$ and (b) downstream with a finite ρ. The coast has a vertical sidewall. The current moves downstream at speed $u(y)$ with the coast on its right, $h(y)$ is the depth of the upper layer, W_0 and w are the upstream and downstream current width, respectively, σ is the density of the upper layer. All the variables are non-dimensionalized.

second equation

$$f - u_y - \frac{u}{\rho + y} = h\delta. \tag{3.2}$$

Equation (3.2) states that the multiplication of the conserved potential vorticity and the current depth (right-hand side) is equal to the total vorticity on the left-hand side, being the sum of the absolute vorticity (the first term) and the relative vorticity (the last two terms, with $u/(\rho + y)$ being the correction term due to curvature).

The variables are non-dimensionalized in the following manner:

$$\begin{aligned} h &= h_0 h' \\ u &= \sqrt{g' h_0}\, u' \\ (x, y) &= R(x', y') \\ \delta &= \frac{f}{h_0}\delta' \end{aligned}$$

where all the primed variables are dimensionless. h_0 is the upstream layer thickness at the wall, and R (defined by $\sqrt{g' h_0}/f$) is the internal Rossby radius of deformation.

Thus the non-dimensional governing equations are

$$u - \frac{u^2}{\rho + y} = -h_y \tag{3.3}$$

$$1 - u_y - \frac{u}{\rho + y} = h\delta, \tag{3.4}$$

where the primes have been dropped from the non-dimensional variables. This is a closed system for the two dependent variables $h(y)$ and $u(y)$.

At the upstream point, with $\rho = \infty$, the centrifugal and curvature terms in equations (3.3) and (3.4) can be dropped. We thus have a set of linear, constant coefficient equations

$$u = -h_y \tag{3.5}$$

$$1 - u_y = h\delta. \tag{3.6}$$

For inviscid, steady-state flow, the Bernoulli function B, defined by

$$B = h + \frac{1}{2}u^2,$$

is conserved along streamlines. This supplies us with two boundary conditions for downstream where ρ is finite:

$$B = B_1 \quad \text{at} \quad y = w \tag{3.7}$$

$$B = B_0 \quad \text{at} \quad y = 0, \tag{3.8}$$

where w is the unknown current width and a function of ρ, B_0 and B_1 are the values of the upstream Bernoulli function at the wall and the offshore edge, respectively. Another boundary condition is

$$h = 0 \quad \text{at} \quad y = w. \tag{3.9}$$

The upstream boundary conditions are

$$h = 1 \quad \text{at} \quad y = 0 \tag{3.10}$$

$$h = 0 \quad \text{at} \quad y = W_0, \tag{3.11}$$

where W_0 is the upstream current width.

The system is governed by two upstream parameters, the potential vorticity δ and the current width W_0. As will be shown later in this chapter, the results do not vary much with δ. Guided by stability analyses (see section 6.1.1), I have chosen $W_0 \in (0.25, 1)$.

3.2 Results

3.2.1 Solutions

We need to solve the system at the upstream point first. Analytical solutions can be found:

$$h(y) = \frac{1}{\delta} + \frac{1}{\delta}\frac{(\delta-1)\sinh[\sqrt{\delta}(W_0-y)] - \sinh[y\sqrt{\delta}]}{\sinh[W_0\sqrt{\delta}]} \tag{3.12}$$

$$u(y) = \frac{1}{\sqrt{\delta}}\frac{(\delta-1)\cosh[\sqrt{\delta}(W_0-y)] + \cosh[y\sqrt{\delta}]}{\sinh[W_0\sqrt{\delta}]}. \tag{3.13}$$

B_0 and B_1 can be obtained according to

$$B_0 = 1 + \frac{1}{2}u^2(0) \tag{3.14}$$

$$B_1 = \frac{1}{2}u^2(W_0). \tag{3.15}$$

Downstream with any particular ρ, equations (3.3) and (3.4) are integrated using a fourth-order Runge-Kutta method with uniform step size (Press et al. 1986). We know that the radius of curvature reaches the critical value ρ_c when the layer thickness at the wall becomes zero, that is, $h(y=0) = 0$. For detailed numerical procedures, see Klinger (1992).

3.2.2 Current Profiles and Critical Curvatures

Typical $h(y)$ and $u(y)$ profiles at both $\rho = \infty$ and $\rho = \rho_c$ are seen in Figure 3.3. Increasing the curvature of the wall, as one travels downstream from a region of zero curvature, decreases the layer thickness at the wall. At some critical radius of curvature ρ_c, the thickness becomes zero, which indicates that separation from the wall occurs. While the upper layer thickness decreases, the velocity increases, but the transport is conserved.

For every pair of (δ, W_0), we can find one critical radius ρ_c. Figure 3.4 shows how ρ_c depends on the upstream parameters δ and W_0: (1) ρ_c decreases as W_0 increases;

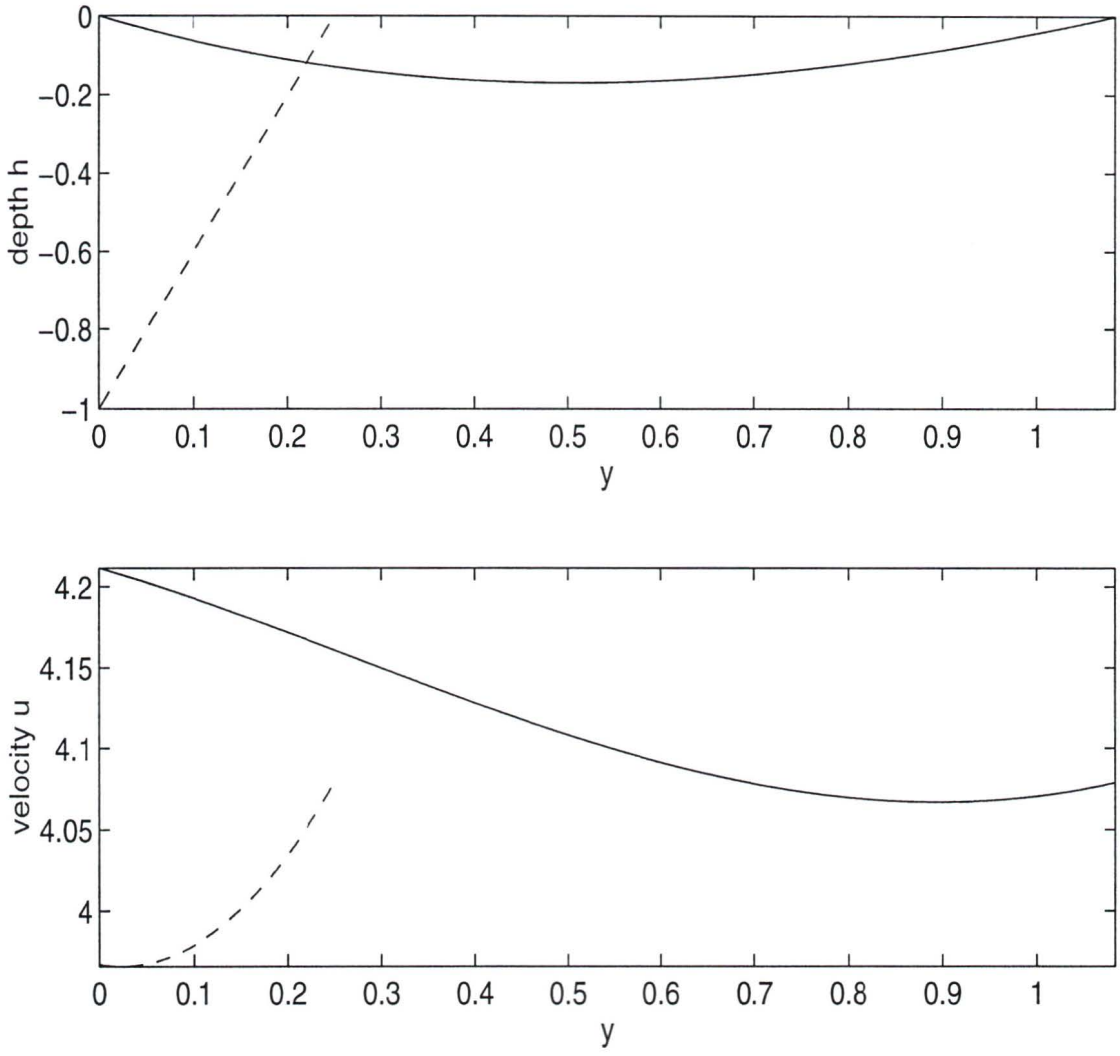

Figure 3.3: Depth and velocity profiles $h(y), u(y)$, for a selected flow ($\delta = 1.1, W_0 = 0.25$), at critical radius of curvature ($\rho = \rho_c$, solid line) and zero curvature ($\rho = \infty$, dashed line). The sidewall at $y = 0$ is vertical.

(2) ρ_c is almost independent of potential vorticity δ. From the figure, we can obtain an approximate relationship between ρ_c and W_0:

$$\rho_c \simeq 0.9/W_0 \qquad \text{for } W_0 \leq 1. \tag{3.16}$$

Now, how is this related to Bormans' and Garrett's (1989) laboratory result $\hat{\rho} < \hat{u}/f$? (Dimensional variables are in hatted form).

Upstream with $\rho = \infty$, the cross-shore momentum equation is $h_y = -u$. Integration with respect to y gives

$$\int_0^{W_0} u\, dy = -\int_0^{W_0} h_y\, dy,$$

thus

$$\overline{u}\, W_0 = h(0) - h(W_0) = 1,$$

and

$$W_0 = 1/\overline{u}. \tag{3.17}$$

The combination of (3.17) with (3.16) yields the model's result for critical radius

$$\rho_c \simeq 0.9\,\overline{u}, \tag{3.18}$$

which, if translated into dimensional form, becomes

$$\hat{\rho}_c \simeq 0.9\,\hat{\overline{u}}/f. \tag{3.19}$$

The agreement with laboratory experiment results is quite good for such a simple model. However, care must be taken in reviewing these solutions because the governing equations (3.1) and (3.2) are derived by neglecting some terms. The consistency of the approximation will be discussed in Chapter 5.

The survey of parameter space undertaken shows that the velocity at the wall is always positive, eliminating flow reversal as the possible mechanism of separation and confirming that the upwelling of the interface is the only mode of separation in this system.

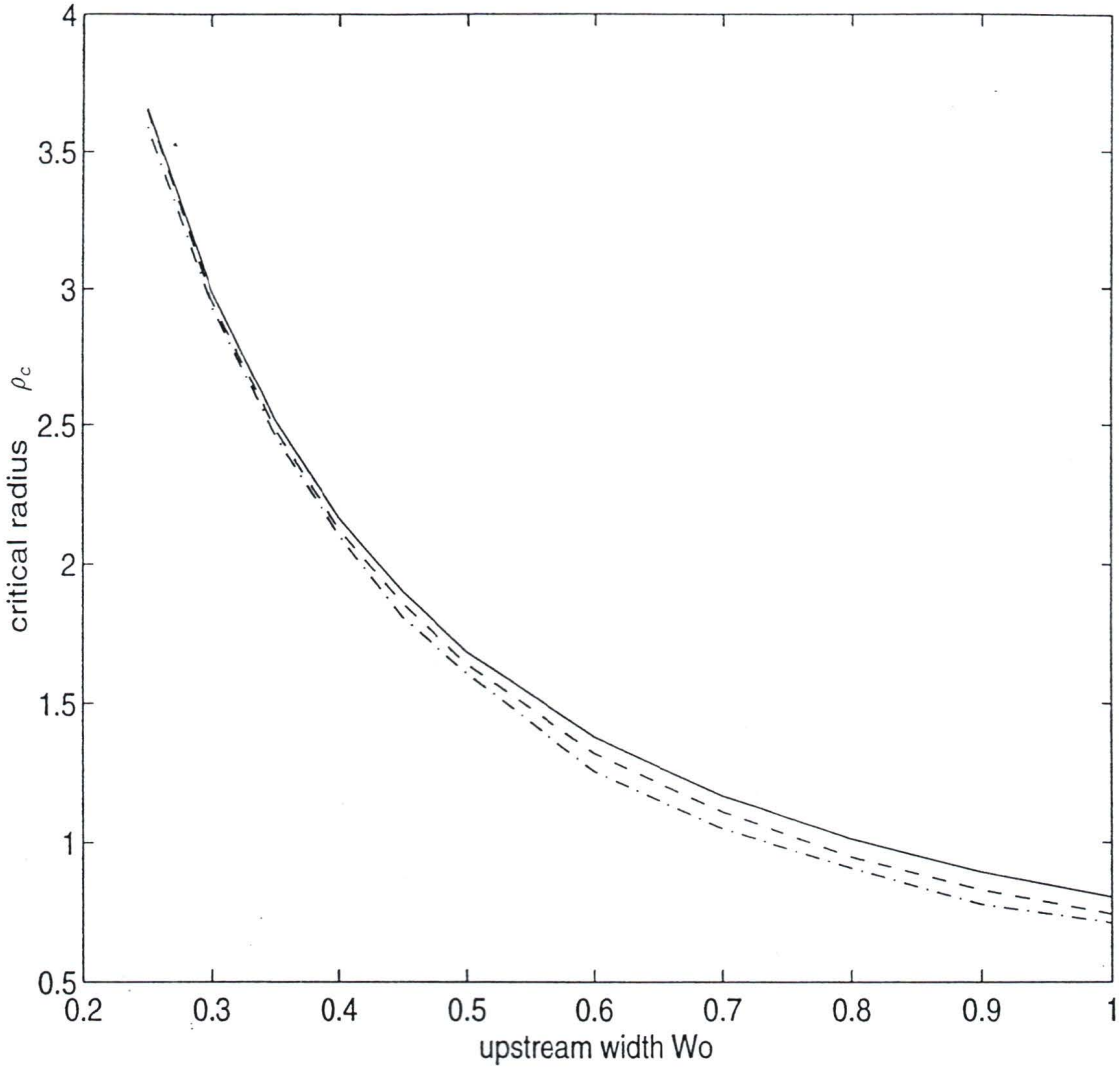

Figure 3.4: The dependence of the critical radius of curvature for separation ρ_c, on upstream width W_0 for different values of upstream potential vorticity δ, $\delta = 1.9$ (solid), 1.1 (dashed), and 0.3 (dash-dotted).

Chapter 4

Interfacial-Upwelling Separation (Sloping Case)

In Klinger's (1994) model, the sidewall of the coast is vertical. In the real world, the coast usually has a sloping side. Thus I seek to improve the model by using a sloping wall instead of a vertical one.

4.1 Governing Equations

The notations used are the same as in the vertical case unless otherwise indicated.

Figure 4.1 shows the cross-sections of the current when the coast has a sloping wall (a) upstream with $\rho = \infty$ and (b) near the corner with a finite ρ. Due to the presence of the slope, the upper layer is divided into two regions: the free region (between the offshore edge and $y = y^*$ where the interface intersects the wall) and the wedge region (between the shore and $y = y^*$). W_0, the upstream width of the free region, is a parameter, while w, the total downstream current width, is unknown and needs to be solved. The upstream thickness at the intersection point is used as the scale for the non-dimensionalization of layer thickness, all other scales are

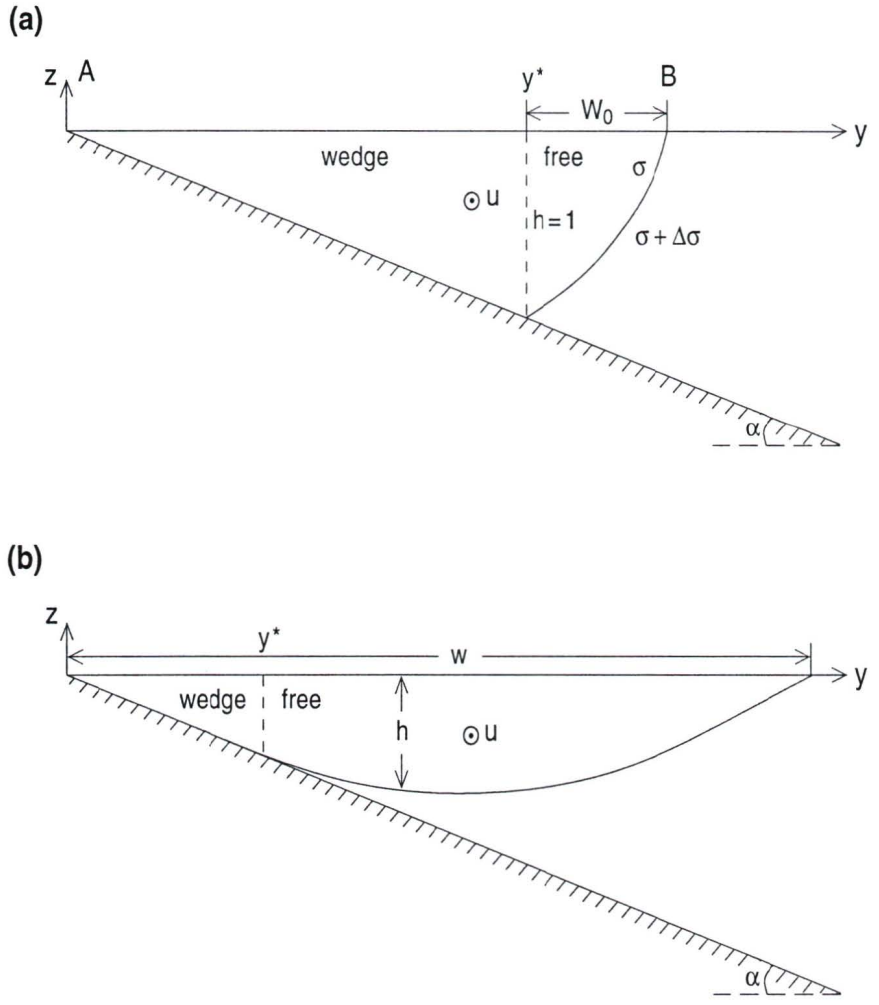

Figure 4.1: Cross-sections of the current in a reduced gravity model (a) upstream with $\rho = \infty$, (b) downstream where ρ is finite. The sidewall of the coast has a slope s ($s = \tan\alpha$). The upper layer is divided into the wedge and free region at y^*, the point where the interface intersects the sloping wall. The current moves downstream at speed $u(y)$ with the coast on its right, $h(y)$ is the upper layer thickness of the free region, w in (b) is the total current width, unknown and a function of ρ. The upstream current width of the free region W_0 is a parameter. All the variables are non-dimensionalized.

defined as in the vertical case.

The cross-shore momentum equation and the potential vorticity equation for the free region are the same as in the vertical case, so that,

$$u - \frac{u^2}{\rho + y} = -h_y \tag{4.1}$$

$$1 - u_y - \frac{u}{\rho + y} = h\delta, \tag{4.2}$$

where $h(y)$ and $u(y)$ are the depth and velocity of the upper layer, respectively, at the point where the radius of curvature is ρ, and are the dependent variables to be solved. For the wedge region, the governing equations are a little different, because the upper layer depth is no longer some variable $h(y)$, but sy, where s is the non-dimensionalized slope, derived from the physical slope s_0 according to

$$s = \frac{s_0}{h_0/R}. \tag{4.3}$$

The pressure gradient in the momentum equation is no longer h_y and has to be changed accordingly. Hence, the equations for the wedge region are

$$u - \frac{u^2}{\rho + y} = -p_y \tag{4.4}$$

$$1 - u_y - \frac{u}{\rho + y} = sy\delta, \tag{4.5}$$

where $p(y)$ is the non-dimensionalized pressure of the wedge region.

The governing equations are simplified upstream because $\rho = \infty$. Thus, they are

$$u = -h_y \tag{4.6}$$

$$1 - u_y = h\delta, \tag{4.7}$$

for the free region and

$$u = -p_y \tag{4.8}$$

$$1 - u_y = sy\delta \tag{4.9}$$

for the wedge region.

The boundary conditions for places with finite ρ are

$$h = 0 \quad \text{at} \quad y = w \tag{4.10}$$

$$\frac{1}{2}u^2 = B_1 \quad \text{at} \quad y = w \tag{4.11}$$

$$p + \frac{1}{2}u^2 = B_0 \quad \text{at} \quad y = 0, \tag{4.12}$$

where w is the unknown current width and a function of ρ, B_0 and B_1 are the upstream values of the Bernoulli function at the wall and the offshore edge respectively. Notice that in the wedge region, the Bernoulli function is defined by $B = p + \frac{1}{2}u^2$.

Upstream, the boundary conditions for the free region are

$$h = 1 \quad \text{at} \quad y = \frac{1}{s} \tag{4.13}$$

$$h = 0 \quad \text{at} \quad y = \frac{1}{s} + W_0, \tag{4.14}$$

where W_0 is the upstream width of the free region. The pressure and velocity of the two regions are matched at the intersection point, $y = 1/s$, which supplies us with the boundary conditions for the wedge region,

$$p\left(\frac{1}{s}\right) = h_m \tag{4.15}$$

$$u\left(\frac{1}{s}\right) = u_m, \tag{4.16}$$

where subscript m denotes the intersection point upstream. $h_m = 1$, u_m can be obtained from the free region solution at $y = 1/s$.

Thus, upstream, the free region is almost identical to the vertical case, in the sense that they have the same governing equations and the same width W_0 at the surface. They also both have $h = 1$ and $h = 0$ on the two boundaries respectively. So the sloping case is really the vertical case with an extra wedge region attached to it. The cross-sectional area of the wedge region at the upstream point is $1/(2s)$.

Thus the smaller s is, the larger the wedge region we have to start with, the more dominant it is over the free region, and the more difference there is between the sloping and vertical cases. On the other hand, if $s \to \infty$, the sloping case should relax to the vertical case.

The system is governed by three parameters: the slope s, the upstream potential vorticity δ and the upstream width W_0 of the free region.

4.2 Results

4.2.1 Solutions

We need to solve the system at the upstream point first.

In the free region, that is, $(1/s) \leq y \leq (1/s + W_0)$, the analytical solutions are almost the same as (3.12) and (3.13) in the vertical case except that y is replaced by $(y - 1/s)$:

$$h(y) = \frac{1}{\delta} + \frac{1}{\delta}\frac{(\delta - 1)\sinh[\sqrt{\delta}(W_0 - y + 1/s)] - \sinh[(y - 1/s)\sqrt{\delta}\,]}{\sinh[W_0\sqrt{\delta}\,]} \quad (4.17)$$

$$u(y) = \frac{1}{\sqrt{\delta}}\frac{(\delta - 1)\cosh[\sqrt{\delta}(W_0 - (y - 1/s))] + \cosh[(y - 1/s)\sqrt{\delta}\,]}{\sinh[W_0\sqrt{\delta}\,]}. \quad (4.18)$$

In the wedge region, that is, $0 \leq y \leq (1/s)$, the solutions are

$$p = \frac{1}{6}\delta s y^3 - \frac{1}{2}y^2 - c_1 y + c_2 \quad (4.19)$$

$$u = -\frac{1}{2}\delta s y^2 + y + c_1, \quad (4.20)$$

where

$$c_1 = u_m + \frac{(\delta/2 - 1)}{s} \quad (4.21)$$

$$c_2 = 1 - \frac{\delta - 3}{6s^2} + \frac{c_1}{s} \quad (4.22)$$

$$u_m = \frac{1}{\sqrt{\delta}}\frac{(\delta - 1)\cosh[W_0\sqrt{\delta}] + 1}{\sinh[W_0\sqrt{\delta}\,]}. \quad (4.23)$$

Downstream, for a particular ρ, we make a guess of the current width w, and start the integration from the outer edge $y = w$ using a fourth-order Runge-Kutta method. The equations are those of the free region (4.1) and (4.2); the boundary conditions are (4.10) and (4.11). The integration goes backwards towards the wall ($y = 0$) until the interface intersects the wall at $y = y^*$ ($h^* = sy^*$) (Figure 4.1), then it switches to equations of the wedge region (4.4) and (4.5). The boundary conditions at the intersection point y^* are

$$u = u^* \qquad \text{at} \quad y = y^* \tag{4.24}$$

$$p = h^* \qquad \text{at} \quad y = y^*, \tag{4.25}$$

where superscript * denotes value at $y = y^*$.

Then, we need to check if the Bernoulli function $B = p + \frac{1}{2}u^2$ is conserved at the shore $y = 0$, which is a streamline. That is, we check if

$$B = p + \frac{1}{2}u^2 = B_0 \qquad \text{at} \quad y = 0 \tag{4.26}$$

is satisfied, where B_0 is the upstream value of the Bernoulli function at $y = 0$. If so, the guess of w for this ρ is right, and the $h(y), u(y)$ and $p(y)$ fields have been determined. Otherwise, depending on whether B is greater or less than B_0, we decrease or increase w and repeat the above procedure.

4.2.2 Current Profiles and Critical Curvatures

Current Profiles

Typical profiles of $h(y)$ and $u(y)$, at both the upstream point (dashed lines) and the critical point of separation (solid lines) are shown in Figure 4.2, with $s = 0.5, \delta = 1.1$ and $W_0 = 0.25$. Basically the upper layer becomes shallower and wider, while the current becomes faster. With all these changes, the cross-sectional transport is conserved.

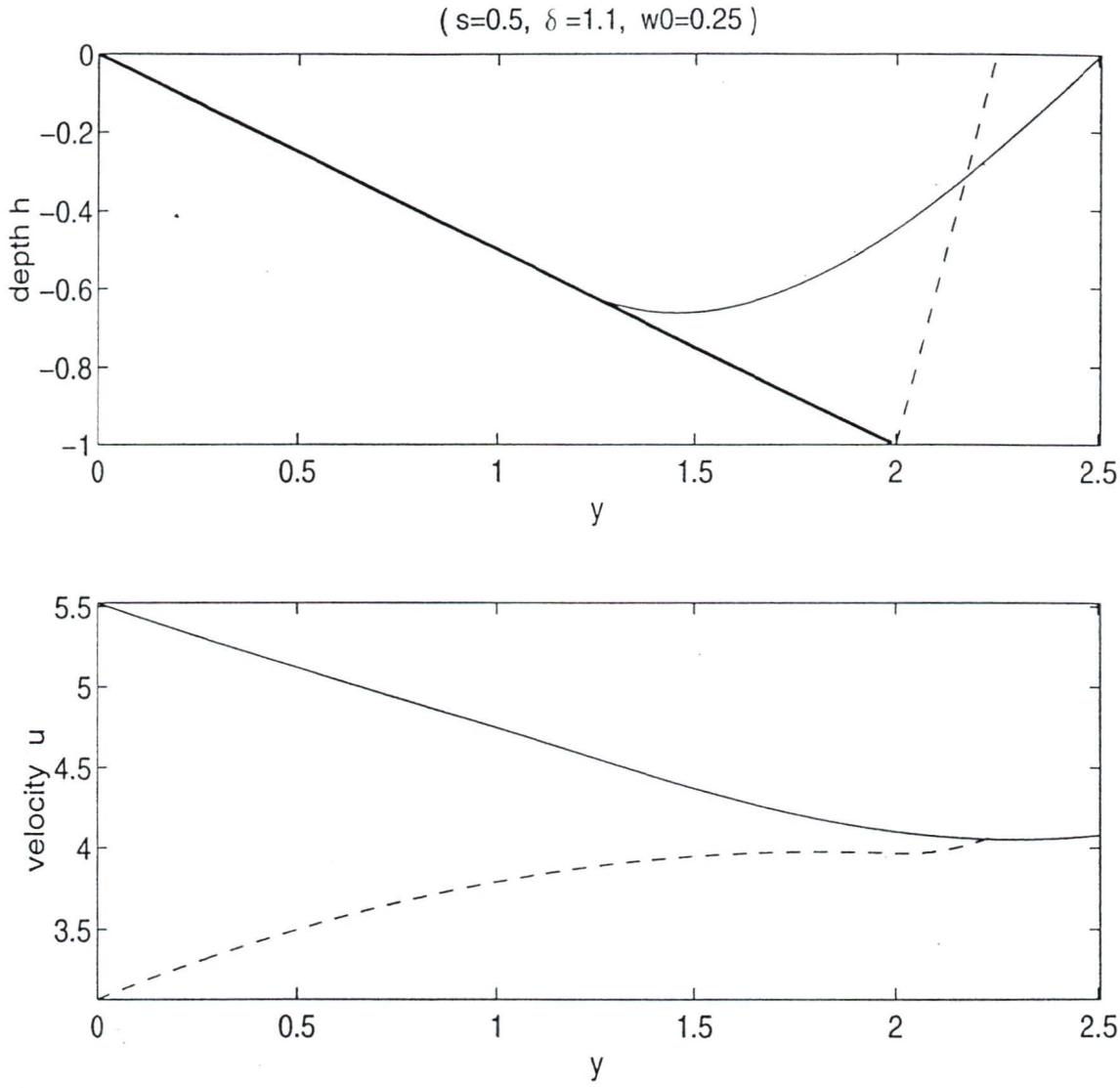

Figure 4.2: Depth and velocity profiles $h(y), u(y)$ for a selected flow ($s = 0.5$, $\delta = 1.1$, $W_0 = 0.25$), with critical radius of curvature ($\rho = \rho_c$, solid line) and zero curvature ($\rho = \infty$, dashed line). The thick line in the depth profile indicates the sloping wall.

The dependence of the profiles on slope s is seen in Figure 4.3, where three cases, with the same δ, W_0, ($\delta = 1.1, W_0 = 0.35$), but different s, ($s = \infty, 1$ and 0.3, respectively) are put together. With a smaller value of s, the most obvious feature is that the current speeds up at the separation point much more than in the vertical case, especially close to the wall. A less dramatic feature is that the upper layer does not spread out as much compared to the vertical case. It is worth mentioning that when s is very small, these effects are so significant that the upper layer actually becomes narrower when it reaches the separation point as opposed to becoming wider as in most cases. This is accompanied by a huge increase in speed near the coast (Figure 4.4).

The profiles also vary with W_0. Figure 4.5 shows two cases with the same s, δ, ($s = 0.5, \delta = 1.1$), but different W_0 (0.25 and 0.5, respectively). The most obvious feature is the large difference in the average upstream velocities, close to 4 for $W_0 = 0.25$ but only 2 for $W_0 = 0.5$. The increase in speed near the coast, accompanied by less spreading out in the h profile, is more obvious for the case with a larger W_0.

Finally, the dependence of the profiles on δ is shown in (Figure 4.6). Three cases are compared, with the same s and W_0 ($s = 0.5, W_0 = 0.25$), but different δ ($\delta = 0.3, 1.1, 1.9$). The h profile does not change much at all, while u increases noticeably with the increase of δ.

Critical Radius

The critical radius of curvature ρ_c is a function of s, δ and W_0. In order to compare results with the vertical case, I focus on how $\rho_c(W_0)$, the relationship between ρ_c and W_0, varies with the slope s. This is shown in Figure 4.7. For $s \geq 2$, the function is almost identical to that of the vertical case ($s = \infty$); for $s < 2$, ρ_c decreases with

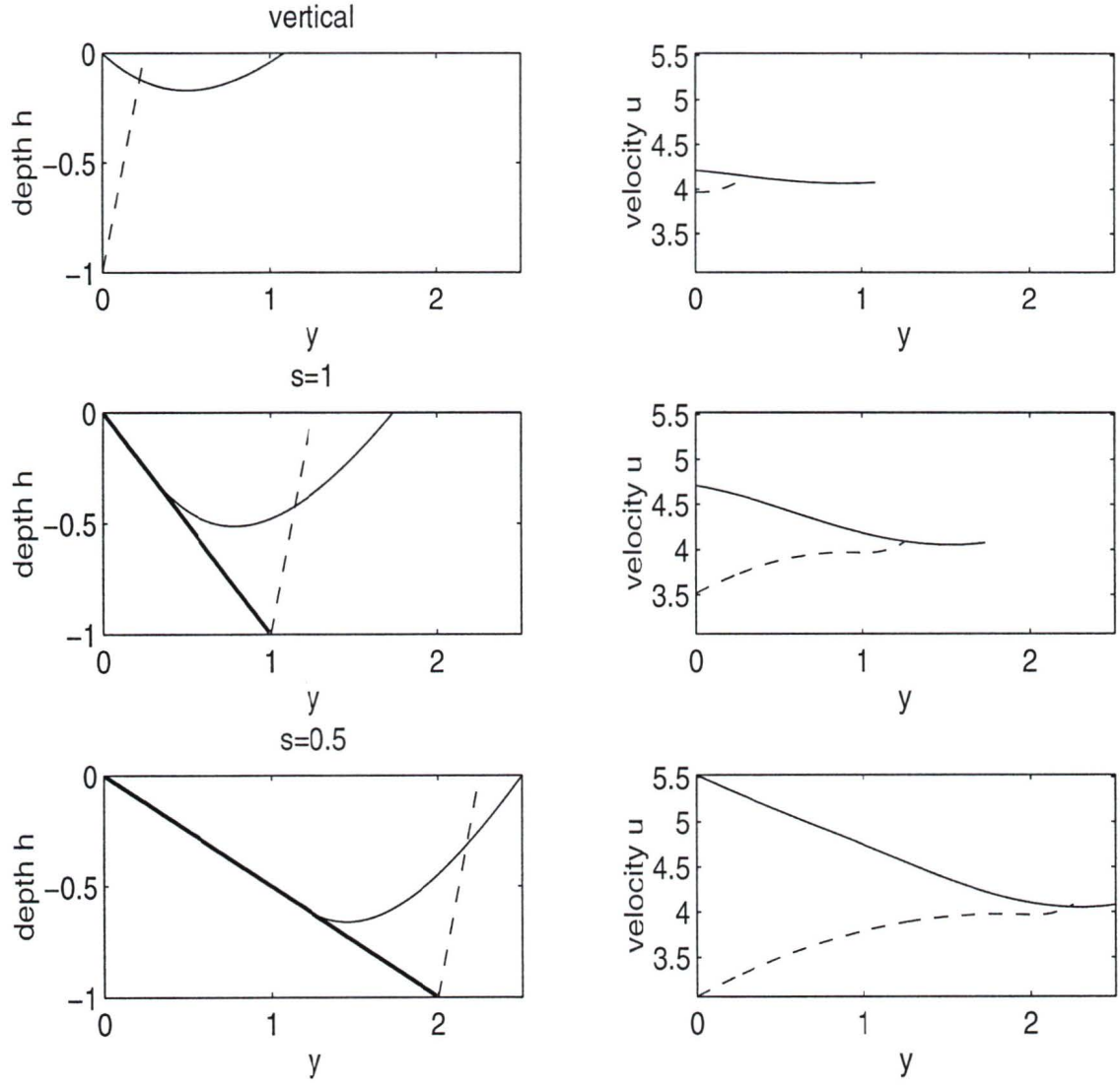

Figure 4.3: Depth and velocity profiles $h(y), u(y)$ for different values of s. In all three figures, $\delta = 1.1, W_0 = 0.25$.

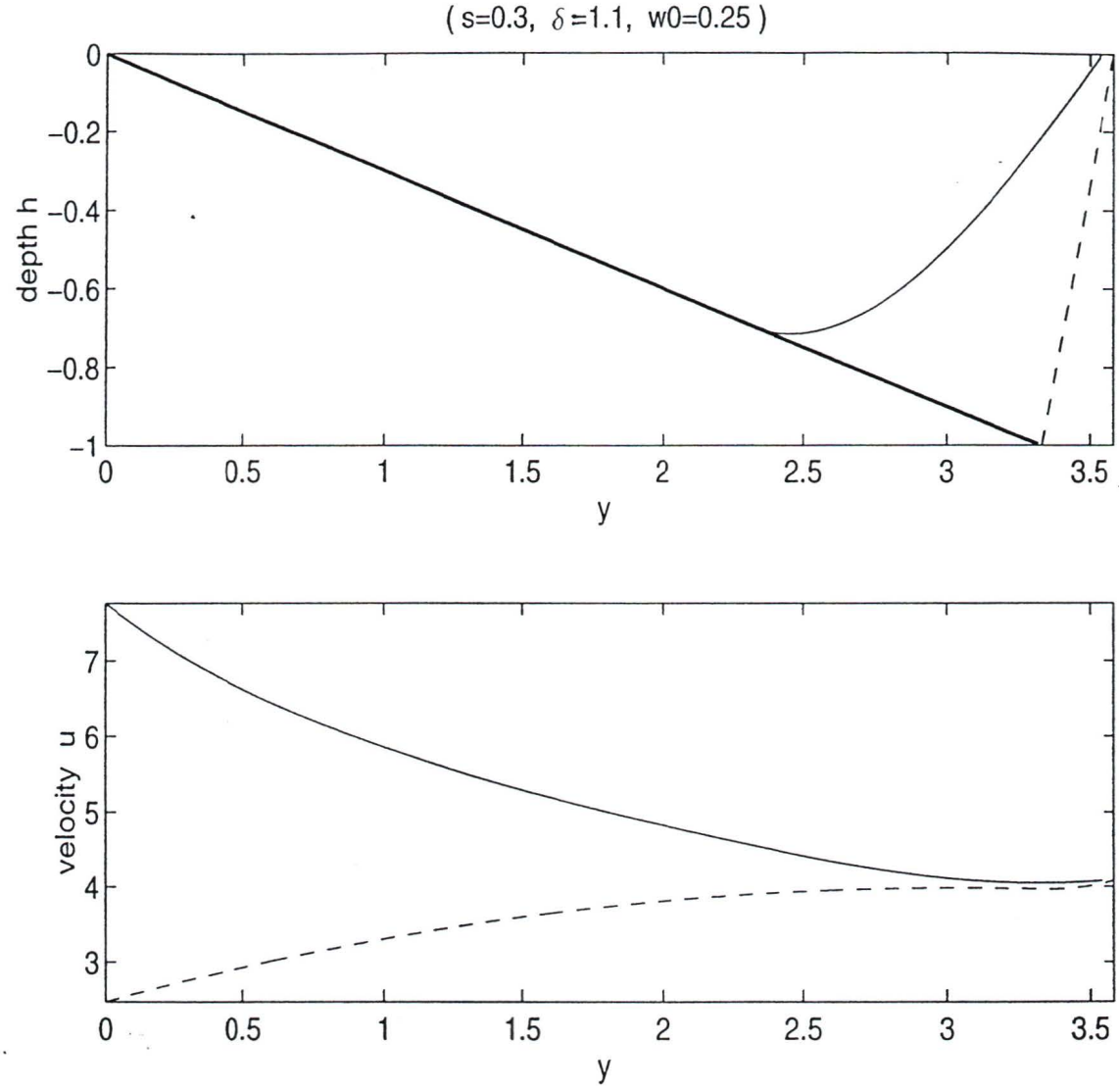

Figure 4.4: When s is very small, the current speeds up significantly close to the shore and the upper layer actually becomes narrower at the upstream point (dashed line) than at the separation point (solid line) ($s = 0.3, \delta = 1.1$, $W_0 = 0.25$). Thick line in the depth profile indicates the sloping wall.

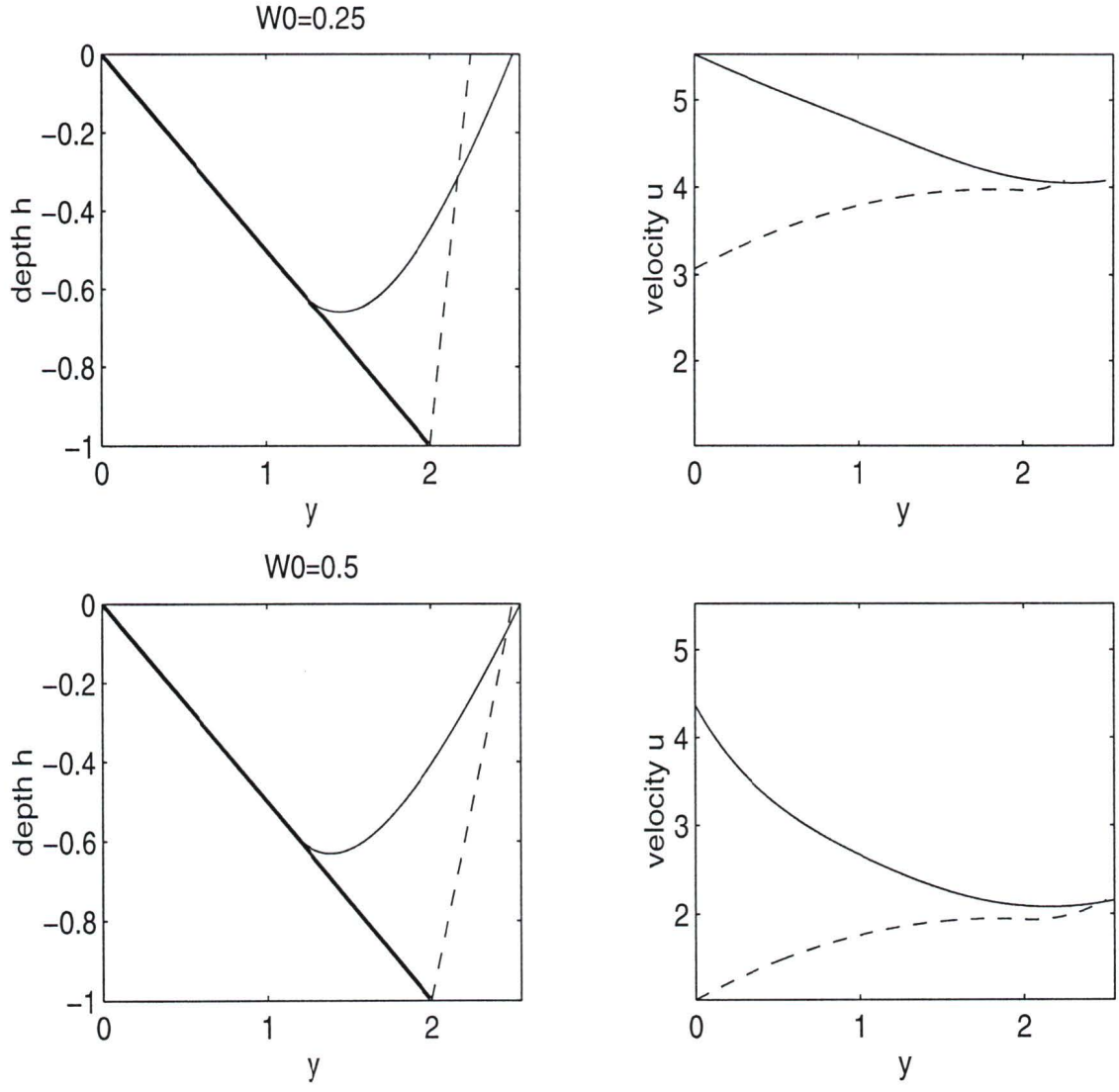

Figure 4.5: Depth and velocity profiles $h(y), u(y)$ for different values of W_0. In both figures, $s = 0.5, \delta = 1.1$.

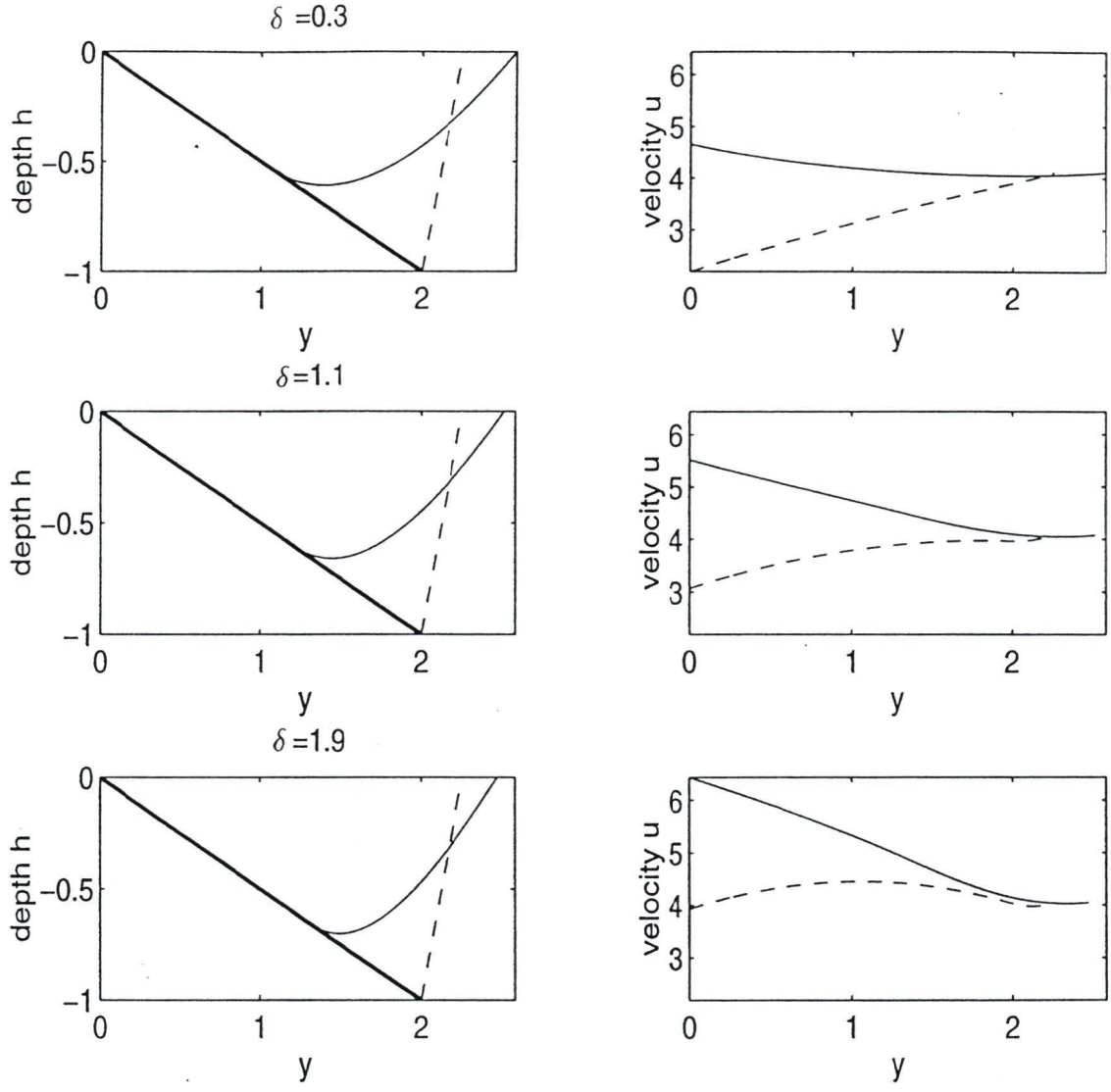

Figure 4.6: Depth and velocity profiles $h(y), u(y)$ for different values of δ. In all three figures, $s = 0.5, W_0 = 0.25$.

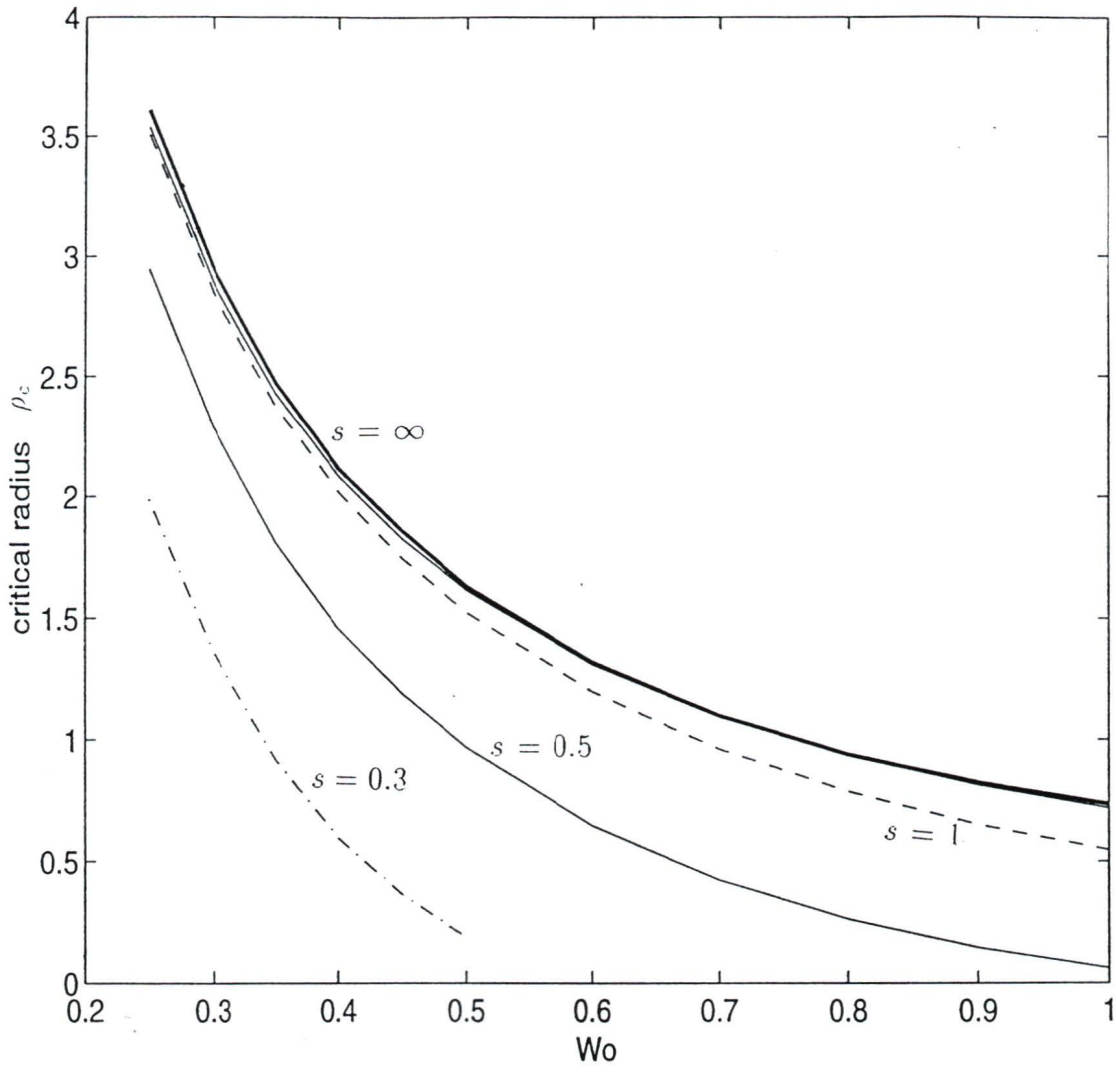

Figure 4.7: The dependence of the critical radius of curvature for separation ρ_c, on W_0, for different values of s. $s = \infty$ (thick line), $s = 2$ (solid line and almost identical to $s = \infty$), $s = 1$ (dashed line), $s = 0.5$ (solid line) and $s = 0.3$ (dash-dotted line). In all cases, $\delta = 1.1$.

a decrease of s. The relationships between ρ_c and upstream width $W_0 + 1/s$ do not collapse for different s, nor do those between $\rho_c + 1/s$ and W_0. For a parrticular s, the empirical relationship between ρ_c and W_0 can be found. For example, for $s = 0.5$, we have

$$\rho_c \simeq 0.9/W_0 - 0.7. \tag{4.27}$$

Since $1/W_0 = \overline{u}_f$, and $\overline{u}_f \simeq \overline{u}$ ($\overline{u}_f$ and $\overline{u}$ are the average upstream velocities in the free and whole regions, respectively), (4.27) gives

$$\rho_c \simeq 0.9\overline{u} - 0.7, \tag{4.28}$$

which corresponds to a dimensional relationship

$$\hat{\rho}_c \simeq 0.9\,\hat{\overline{u}}/f - 0.7\hat{R}. \tag{4.29}$$

For a particular W_0, cases with different s have the same upstream *free* regions: the width being W_0 and the layer depth at the intersection point being 1, which corresponds to the vertical counterpart. It is the attached wedge regions that vary in slopes. Upstream, the wedge region has a width of $1/s$ and a cross-sectional area of $1/2s$. Hence, the wedge region gets larger as the slope s gets smaller. With the model set up this way, the current generally requires a greater curvature of the sloping coast than of its vertical counterpart in order to separate.

As in the vertical case, generally, the results do not depend greatly on δ. However, the dependence may be magnified in cases with smaller values of s (say, less than 1), though still quite small (Figure 4.8).

Again, the survey of parameter space undertaken shows that velocity at the wall is always positive, eliminating flow reversal as the possible mechanism of separation and confirming that the upwelling of the interface is the only mode of separation in this system.

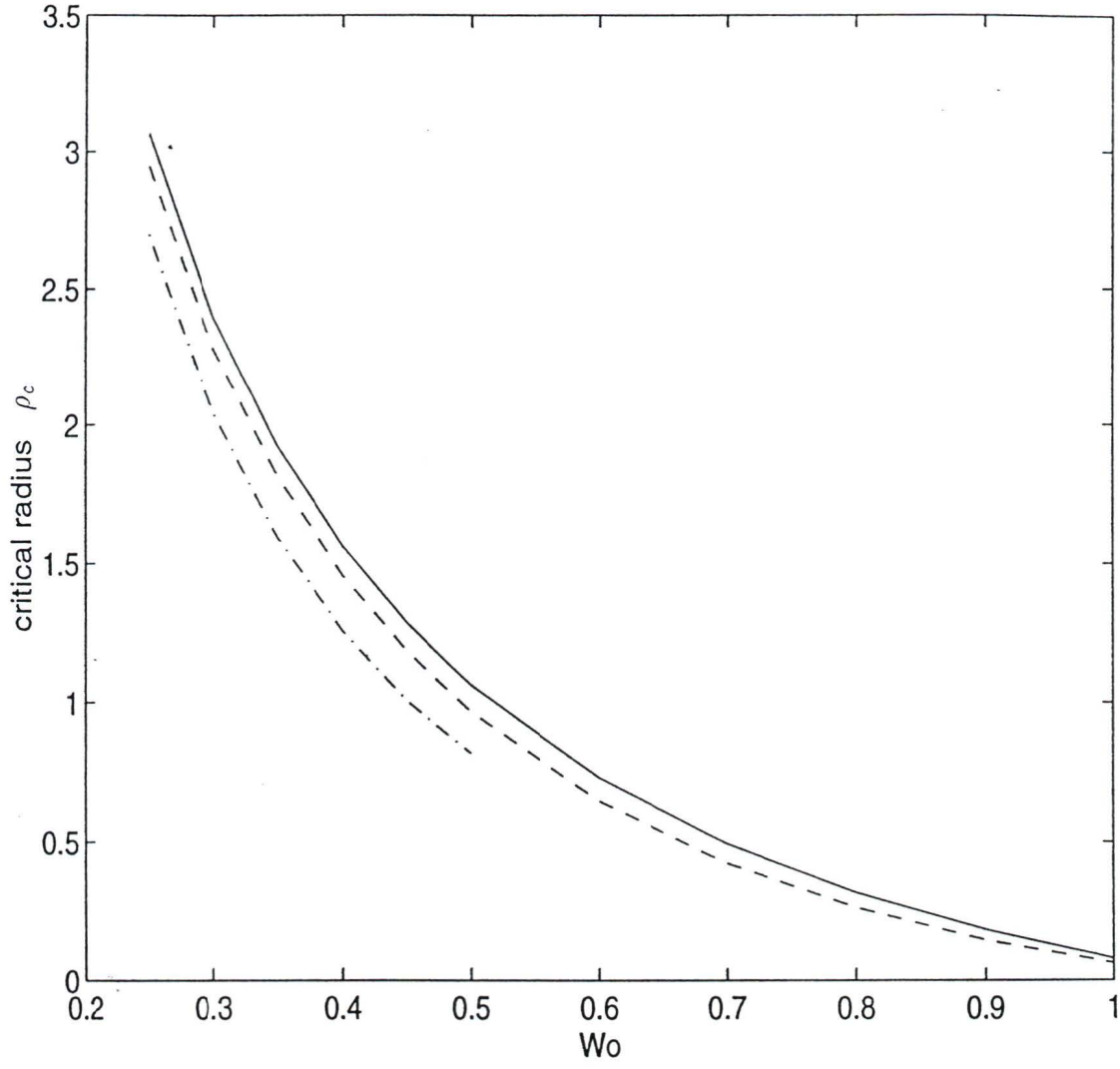

Figure 4.8: The dependence of the critical radius of curvature for separation ρ_c, on W_0 for different values of δ. $\delta = 1.9$ (solid), 1.1 (dashed) and 0.3 (dash-dotted). In all cases, $s = 0.5$.

Chapter 5

Consistency of the Approximation

In both the vertical and sloping cases, we have assumed that the alongshore variation length scale is long compared to the cross-shore one. Thus, we are able to neglect some terms and reduce the partial differential equations into ordinary differential equations with respect to the cross-shore coordinate y only. Now that we have solved these simplified equations, we should check if this approximation is consistent, that is, if the neglected terms are indeed small compared to the retained terms.

5.1 Vertical Case

The non-dimensionalized cross-shore momentum equation and potential vorticity equation before approximation (following Røed 1980) are

$$\underline{\frac{u\,v_x}{1+y/\rho}} + \underline{v\,v_y} + u - \frac{u^2}{\rho+y} = -h_y \tag{5.1}$$

$$1 + \underline{\frac{v_x}{1+y/\rho}} - u_y - \frac{u}{\rho+y} = \delta h, \tag{5.2}$$

with the neglected terms underlined.

To determine the magnitude of these neglected terms, we need to know v, which

appears in the alongshore momentum equation (Røed 1980)

$$\frac{uu_x}{1+y/\rho} + \left(u_y + \frac{u}{\rho+y} - 1\right) v = -\frac{h_x}{1+y/\rho}. \tag{5.3}$$

The h and u obtained by integrating equations (3.3) and (3.4) are used to calculate v, which is derived by combining equation (3.4) and (5.3), so that,

$$v = \frac{1}{\delta h}\left(\frac{h_x + uu_x}{1+y/\rho}\right). \tag{5.4}$$

We also need to choose a specific curvature profile $\rho(x)$ so that we can convert the fields of $[u(\rho,y), v(\rho,y), h(\rho,y)]$ to $[u(x,y), v(x,y), h(x,y)]$ and thus calculate the x derivatives. The $\rho(x)$ we choose (after Klinger (1994)) is

$$\rho(x) = \rho_M \exp[4(x/\rho_M)^2/\pi], \tag{5.5}$$

where ρ_M is the radius of curvature at the corner, $x = 0$. The numerical factors ensure that the corner is a right angle, as in Bormans and Garrett (1989), that is, the upstream and downstream coastlines far from the corner are at right angles to each other. Equation (5.5) is easily inverted to obtain $x(\rho)$.

The approximation is based on the assumption that the alongshore variation length scale is large compared to that of the cross-shore variations. Since the current spreads out as the curvature increases, the place where the approximation is least likely to be valid is where the coastline has the maximum curvature (minimum ρ), which is the corner $x = 0$ for our chosen coastline. Thus we choose to carry out our test at $x = 0$.

We can tell from (5.5) that ρ is an even function of x. Hence, as long as $\rho_M > \rho_c$ (separation does not occur anywhere), then, $h(\rho)$ and $u(\rho)$ are both symmetrical about $x = 0$, and their derivatives h_x, u_x are zero. Thus according to (5.4), v is zero for all $y's$ at the corner, hence v_y is zero as well. So, we only need to calculate the v_x terms in order to evaluate the neglected terms in (5.1) and (5.2).

By taking the x derivative of (5.4), and using the property of symmetry, v_x at $x = 0$ is

$$v_x = \frac{1}{\delta h}\left(\frac{h_{xx} + uu_{xx}}{1 + y/\rho}\right). \tag{5.6}$$

All derivatives are calculated using a finite-difference approximation (centered-difference method). Thus, the second derivatives are

$$h_{xx} = \frac{h^{-1} - 2h^0 + h^1}{(\Delta x)^2} = \frac{2(h^{-1} - h^0)}{(\Delta x)^2} \tag{5.7}$$

$$u_{xx} = \frac{u^{-1} - 2u^0 + u^1}{(\Delta x)^2} = \frac{2(u^{-1} - u^0)}{(\Delta x)^2}, \tag{5.8}$$

where, superscript 0 denotes the corner $x = 0$, superscripts (-1) and 1 denote Δx upstream and downstream of the corner, respectively. The property of symmetry, $h^{-1} = h^1, u^{-1} = u^1$ has been used. Thus, v_x at $x = 0$ is

$$v_x = \frac{2}{\delta h^0}\frac{(h^1 - h^0) + u^0(u^1 - u^0)}{(1 + y^0/\rho_M)(\Delta x)^2}. \tag{5.9}$$

I set

$$\rho_M = r_m \rho_c \tag{5.10}$$

$$\Delta x = r_x \rho_M, \tag{5.11}$$

where r_m can be any number greater than 1. I choose $r_m = 1.1$ in my test so that the corner has a radius of curvature slightly larger than the critical radius for separation.

The v_x terms are then compared to the reference terms b_r and c_r, which are the maximum of the terms in (5.1) and (5.2) respectively:

$$b_r = \max\left(|h_y|, u, \frac{u^2}{\rho + y}\right) \tag{5.12}$$

$$c_r = \max\left(\frac{u}{\rho + y}, \delta h, 1, |u_y|\right). \tag{5.13}$$

The ratios of $b_3 = (uv_x)/(1 + y/\rho)$ compared to b_r, $c_4 = v_x/(1 + y/\rho)$ to c_r for the case with $\delta = 1.1, W_0 = 0.25$ are shown in Figure 5.1. In a large part of the region across the stream, the ratios are $O(1)$, which means that, close to the critical point, the neglected terms are as important as the retained terms. Figure 5.2 shows that the situation does not improve for other values of δ and W_0. Therefore, overall, for the vertical case, the assumption that the terms involving alongshore derivatives are negligible is not valid close to the separation point.

It is recommended that in future studies, the neglected terms be included and the partial differential equations be solved. However, we can make some qualitative anticipation as to what difference this might bring. The above calculations show that $v_x < 0$ at the corner. Hence, from (5.1), we know b_3 strengthens the centrifugal term which allows separation to occur. Thus, we would expect separation to occur earlier if the neglected terms are included. In (5.2), the effect of including the neglected v_x term will not be as significant, because even if u_y changes by 100%, the velocity u itself will not change very much.

5.2 Sloping Case

Unlike in the vertical case, the layer thickness can no longer be represented by $h(y)$ for all $y's$ at a certain x, because in the wedge region, it is sy instead. A new variable $d(y)$ is defined to represent the layer thickness in both the free and wedge regions:

$$d = \begin{cases} h & \text{in the free region} \\ s\,y & \text{in the wedge region.} \end{cases}$$

This way, we can put the governing equations of both regions together. Hence, the equations before approximation are

$$\underline{\frac{u\,v_x}{1 + y/\rho}} + \underline{v\,v_y} + u - \frac{u^2}{\rho + y} = -p_y \tag{5.14}$$

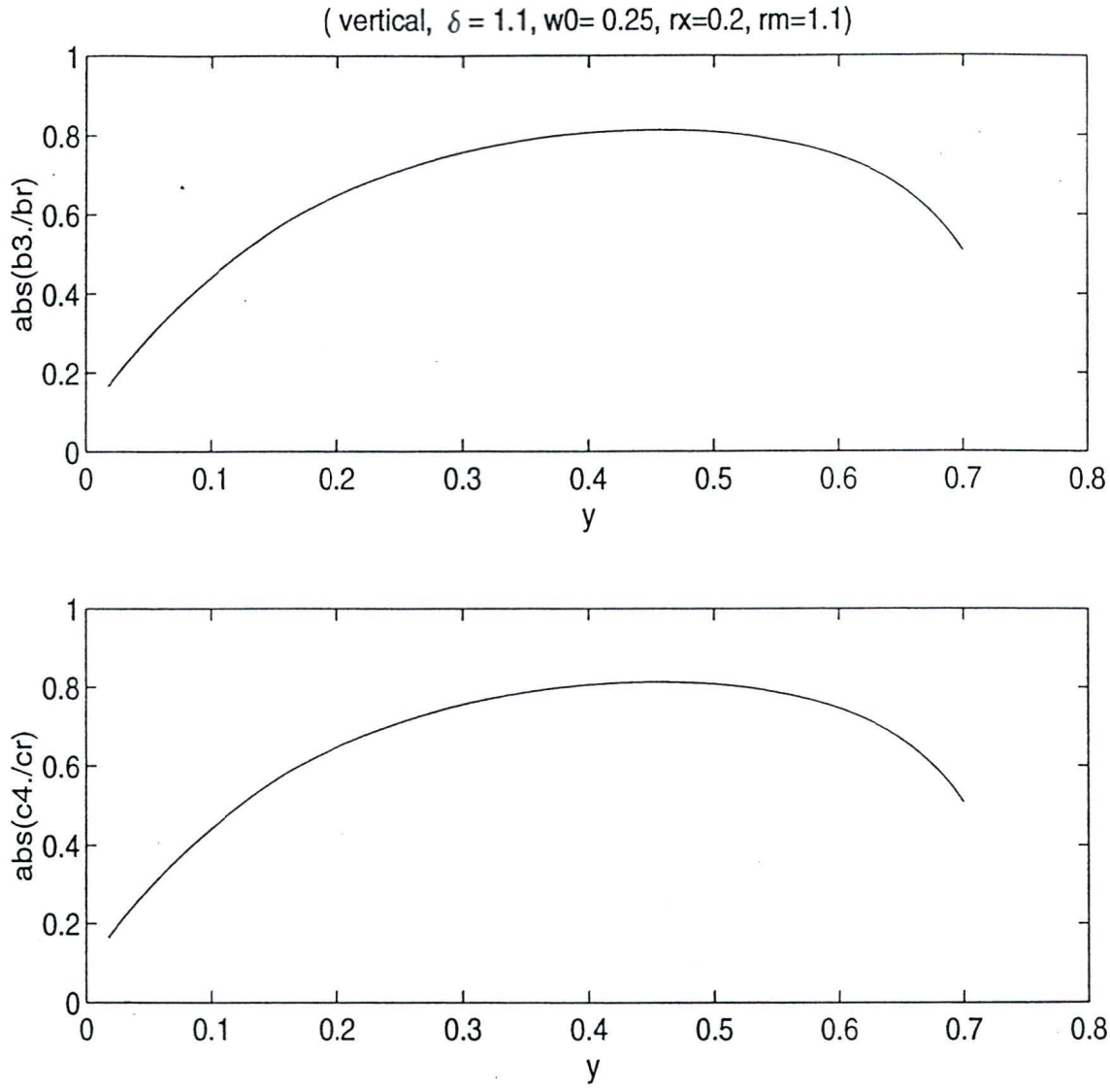

Figure 5.1: The neglected term $b_3 = (uv_x)/(1 + y/\rho)$, is compared to b_r, $c_4 = v_x/(1 + y/\rho)$ to c_r, where b_r and c_r are the maximum of the retained terms in (5.1) and (5.2), respectively. (vertical, $\delta = 1.1, W_0 = 0.25$).

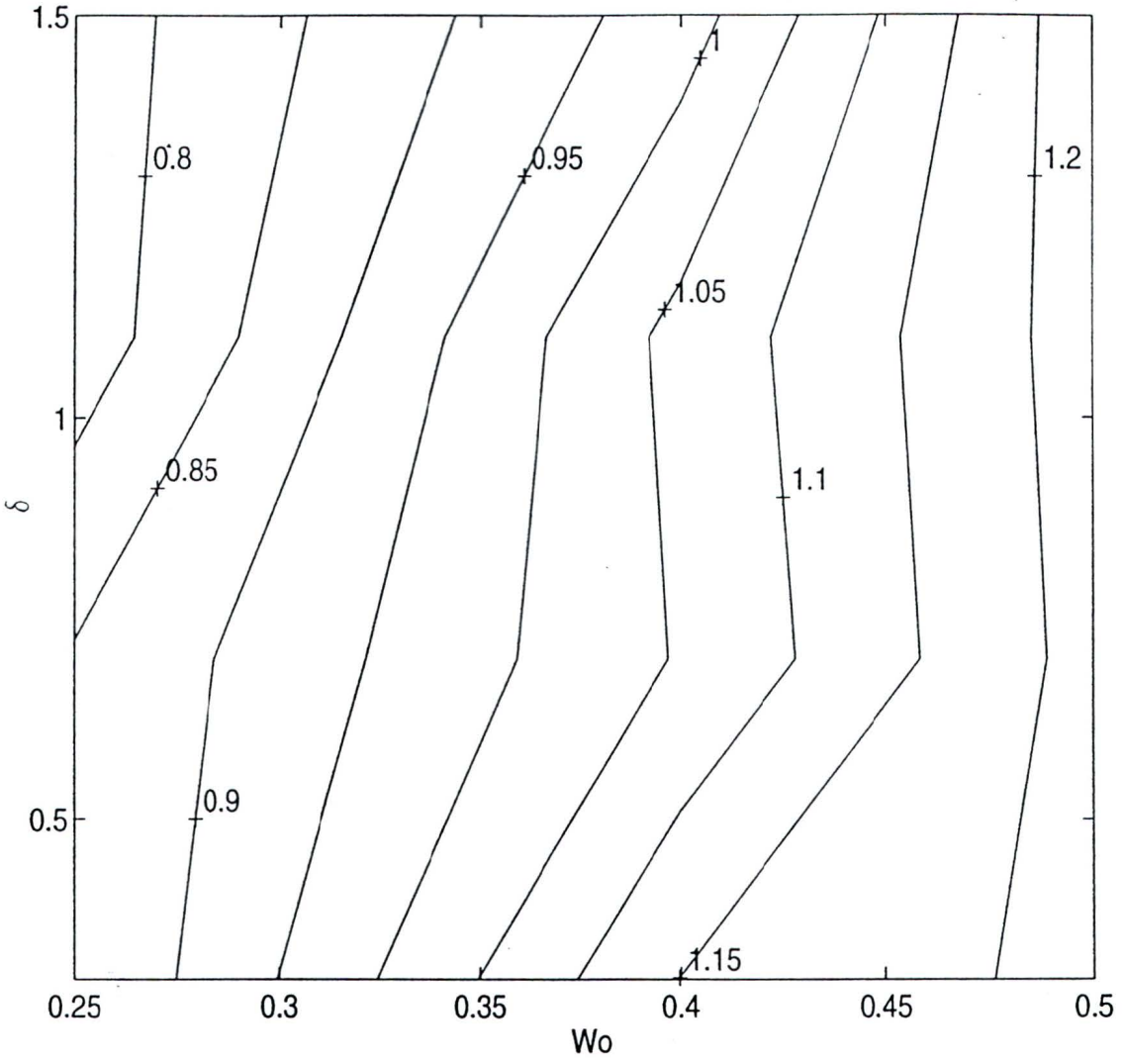

Figure 5.2: The contours of the maximum ratios between $b_3 = uv_x/(1 + y/\rho)$ and the reference b_r, at the corner, where the radius is $\rho_M = 1.1\rho_c$ for different values of δ and W_0. The sidewall at $y = 0$ is vertical.

$$1 + \underline{\frac{v_x}{1+y/\rho}} - u_y - \frac{u}{\rho+y} = \delta d, \tag{5.15}$$

with the neglected terms underlined. p represents the pressure for the whole region and is equal to h in the free region.

Again, we choose to test the consistency of the approximation at the corner, $x = 0$, where the radius of curvature is $\rho_M = r_m \rho_c$ ($r_m > 1$). At this point, we have

$$v = \frac{1}{\delta d}\left(\frac{p_x + u u_x}{1+y/\rho}\right), \tag{5.16}$$

and

$$v_x = \frac{1}{\delta d}\left(\frac{p_{xx} + u u_{xx}}{1+y/\rho}\right). \tag{5.17}$$

The numerical approximation for v_x is

$$v_x = \frac{2}{\delta d^0}\frac{(p^1 - p^0) + u^0(u^1 - u^0)}{(1 + y^0/\rho_M)(\Delta x)^2}, \tag{5.18}$$

where the superscripts have the same meaning as in the vertical case.

Figure 5.3 shows the result for the case with $s = 0.5$ ($\delta = 1.1, W_0 = 0.25$, $r_m = 1.1$). Compared to its vertical counterpart in Figure 5.1, the ratios are much smaller – less than 0.2 as opposed to close to 1. The reason might lie in the fact that the current speeds up significantly in sloping cases, especially with small values of s, so the maximum terms, which, according to calculation, usually are the centrifugal term $u^2/(\rho + y)$ in (5.14) and $u/(\rho + y)$ in (5.15), are much magnified, resulting in smaller ratios.

The ratio b_3/b_r for different slopes and different W_0 is shown in Figure 5.4. The errors decrease with the decrease of s, whereas they do not vary as much with W_0. When $s < 2$, the ratios are less than 0.5, and the assumption can be considered reasonably valid.

Unlike in the vertical case where the current becomes shallower as one travels downstream, the thickness of the current in the wedge region is constant in the

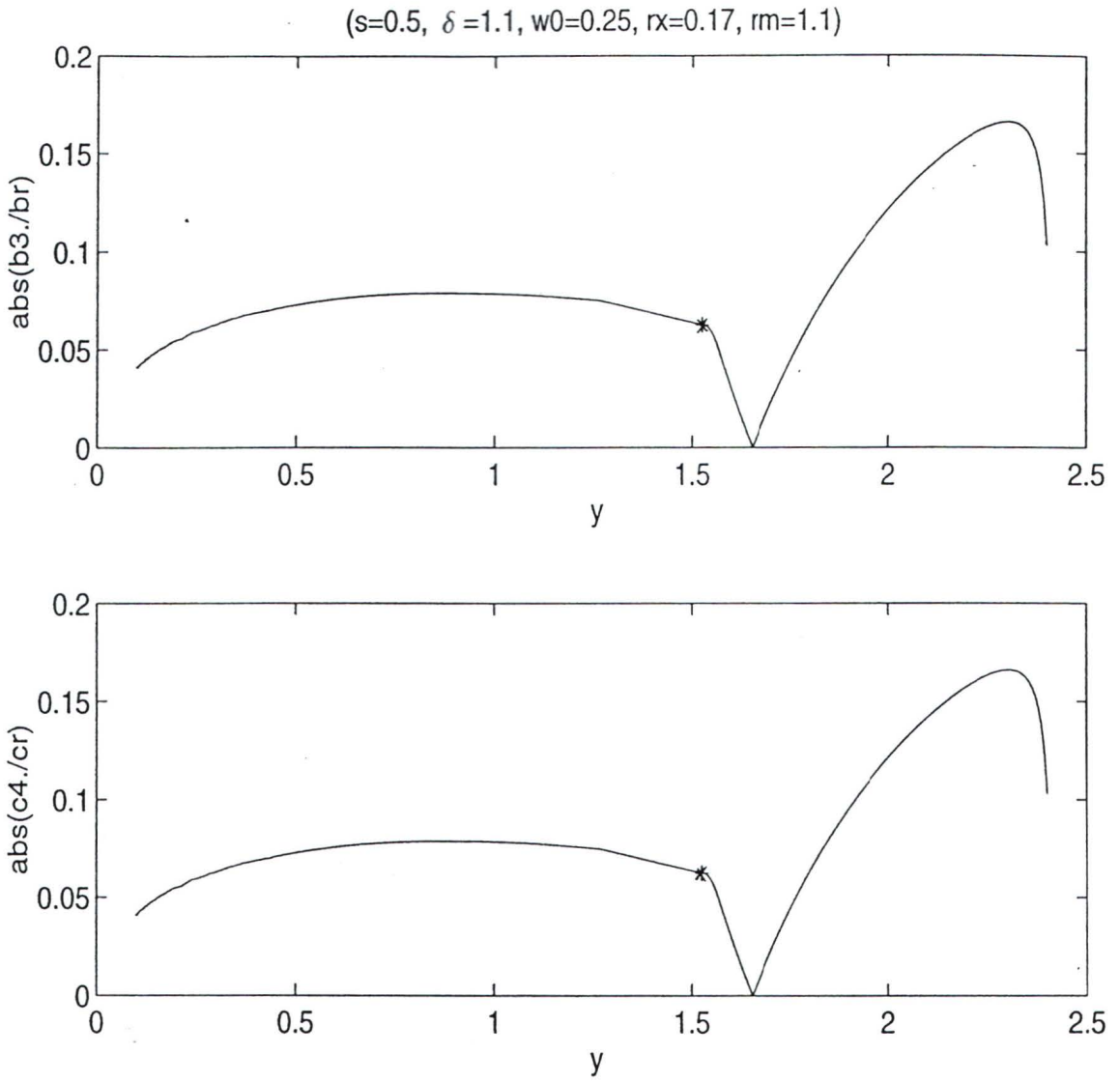

Figure 5.3: The neglected term $b_3 = (uv_x)/(1 + y/\rho)$, is compared to b_r, $c_4 = v_x/(1 + y/\rho)$ to c_r, where b_r and c_r are the maximum of the retained terms in (5.14) and (5.15) respectively. The star signs in the plots indicate the intersection point. $(s = 0.5, \delta = 1.1, W_0 = 0.25)$

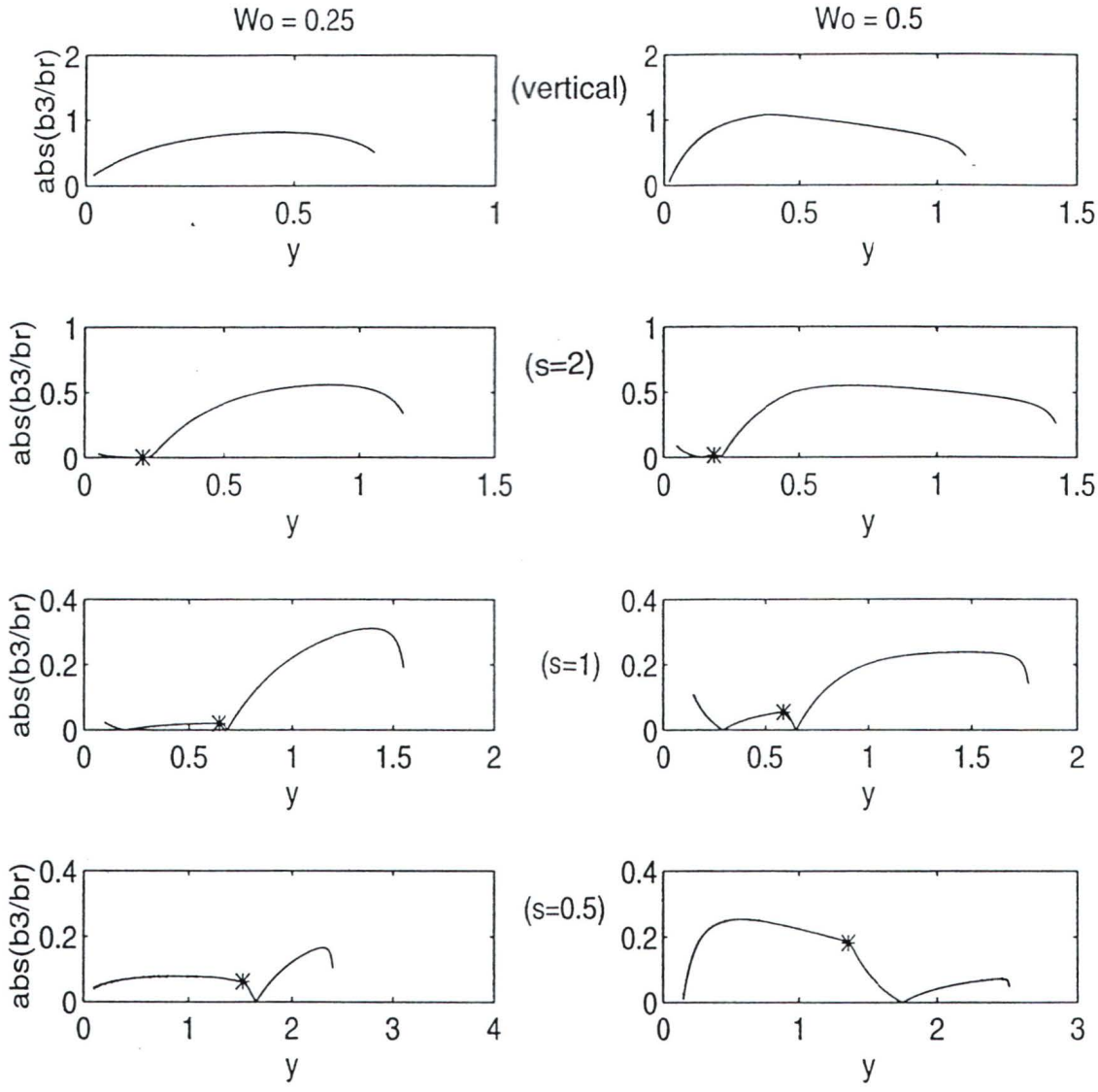

Figure 5.4: Ratios between $b_3 = (uv_x)/(1 + y/\rho)$ and b_r, the maximum of the retained terms in (5.1), for $s = \infty$, 2, 1 and 0.5. $W_0 = 0.25$ for the left column and 0.50 for the right. In all three cases, $\delta = 1.1$. The star signs in the plots indicate the intersection points.

sloping case. According to continuity, $v < 0$ is required upstream of the corner to supply the water necessary for the speeding up of the current. After the corner, $v > 0$. Thus we have $v_x > 0$ at the corner. If we are to include the v_x term in the momentum equation, it will weaken the centrifugal term and delay the occurrence of separation.

Chapter 6

Discussion, Applications and Conclusions

6.1 Discussion

6.1.1 Stability of the current

Now, we need to consider the stability of the currents we have studied, because if they are inherently unstable, they may break into a meandering state before flow separation occurs due to the upwelling of the interface.

Griffiths and Linden (1981) investigated the stability of boundary currents. They generated boundary currents in a two-layer rotating system by continuously supplying buoyant fluid from a source adjacent to the boundary. The currents increased in width and depth to a size at which they became unstable to wave-like disturbances.

This observed instability was successfully described by a simple model for baroclinic instability of a two-layer channel flow, with dissipation at the density interface and arbitrary ratio of layer depths but no horizontal velocity shear. They found that

for a certain depth ratio $\gamma = h_1/h_2$, all wavenumbers are stable until

$$F = \frac{f^2 L^2}{g' h_1} \quad > \quad F_c, \tag{6.1}$$

where L is the current width, F is the Froude number and F_c is a critical value.

F_c is a function of γ, and increases as γ decreases, as shown in Figure 6.1. In our model, the bottom layer is quiescent and infinitely deep, thus $\gamma \to 0$ and the corresponding F_c is $\simeq 36$, where Jones' (1977) result is used because it assumes an inviscid, wedge-shaped boundary current.

Since

$$F = \frac{f^2 L^2}{g' h_1} = \frac{L^2}{g' h_1 / f^2} \quad = \quad \left(\frac{L}{R}\right)^2, \tag{6.2}$$

where R is the internal Rossby radius, the Froude number corresponds to the square of w in our model, where w is the non-dimensionalized current width. Thus, (6.1) is equivalent to $w^2 > 36$. Therefore,

$$w \quad > \quad 6 \tag{6.3}$$

is required for any baroclinic instability to occur. So the baroclinic instability analysis imposes an upper limit for W_0 for the current to be stable. For the parameter space we have chosen to study, the currents are indeed stable.

Note in our model, we have horizontal shear, whose kinetic energy could be the energy source for barotropic instability. But because it is very weak and there is no inflection point within the flow, barotropic instability should not be important.

We examine next the possibility of shear instability of the reduced gravity flow. When the interface is of zero thickness, the flow is always unstable (to short waves). The disturbances will smear out the sharp density and velocity profiles so that the differences now occur over a finite difference Δh. The Richardson number is

$$Ri \quad = \quad \frac{-\frac{g}{\rho}\frac{\Delta\rho}{\Delta h}}{(u/\Delta h)^2} = \frac{g' \Delta h}{u^2}$$

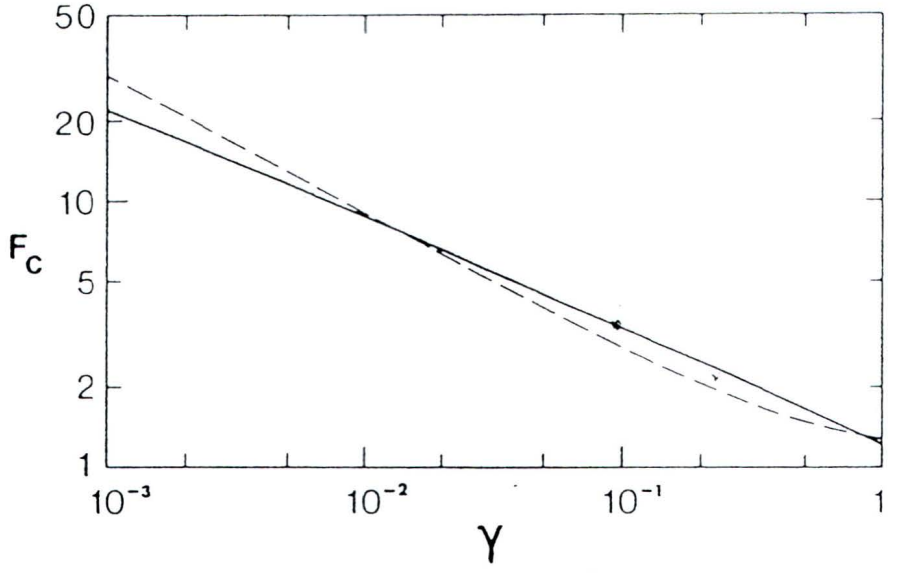

Figure 6.1: The critical Froude number F_c as a function of the depth ratio $\gamma = h_1/h_2$, below which all wavenumbers are stable at any vertical shear. The solid line is given by Griffiths' and Linden's (1981) model where the interface intersects both walls of the channel, and the broken line by a model for a wedge-shaped current with a uniform velocity and a free front (Jones 1977) (after Griffiths and Linden 1981).

$$= \frac{g' h_0}{u^2} \frac{\Delta h}{h_0}$$
$$\simeq {W_0}^2 \frac{\Delta h}{h_0},$$

where h_0 is the upstream layer thickness at the wall, and W_0 is the dimensionless current width. Thus,

$$\frac{\Delta h}{h_0} = \frac{Ri}{{W_0}^2}.$$

Since $\frac{1}{2}\Delta h$ should not exceed h_0, we require

$$W_0 > \sqrt{\frac{Ri}{2}}. \tag{6.4}$$

For the flow to be stable, $Ri > 1/4$, so that

$$W_0 > 0.3, \tag{6.5}$$

for a two-layer model to be meaningful.

6.1.2 Effects of Viscosity

In the chapters discussing the interface upwelling mechanisms, the fluid is assumed inviscid. This is done to simplify the problem and highlight the effect of coastline curvature. One might ask: What if the fluid were viscous? Will flow reversal occur as in the boundary layer separation mechanism? While a friction term could be included in the equations and solved numerically, a simple, qualitative discussion will shed some light.

If the fluid is viscous, then upstream, close to the wall, the velocity should be zero according to the no-slip condition. This can be simulated by manipulating (s, δ, W_0) so that u at the coast is just above zero, though the governing equations are still inviscid (Figure 6.2).

In our model, the flow speeds up greatly as it approaches the corner, especially for slopes of small values, indicating a large *favourable* pressure gradient upstream of the

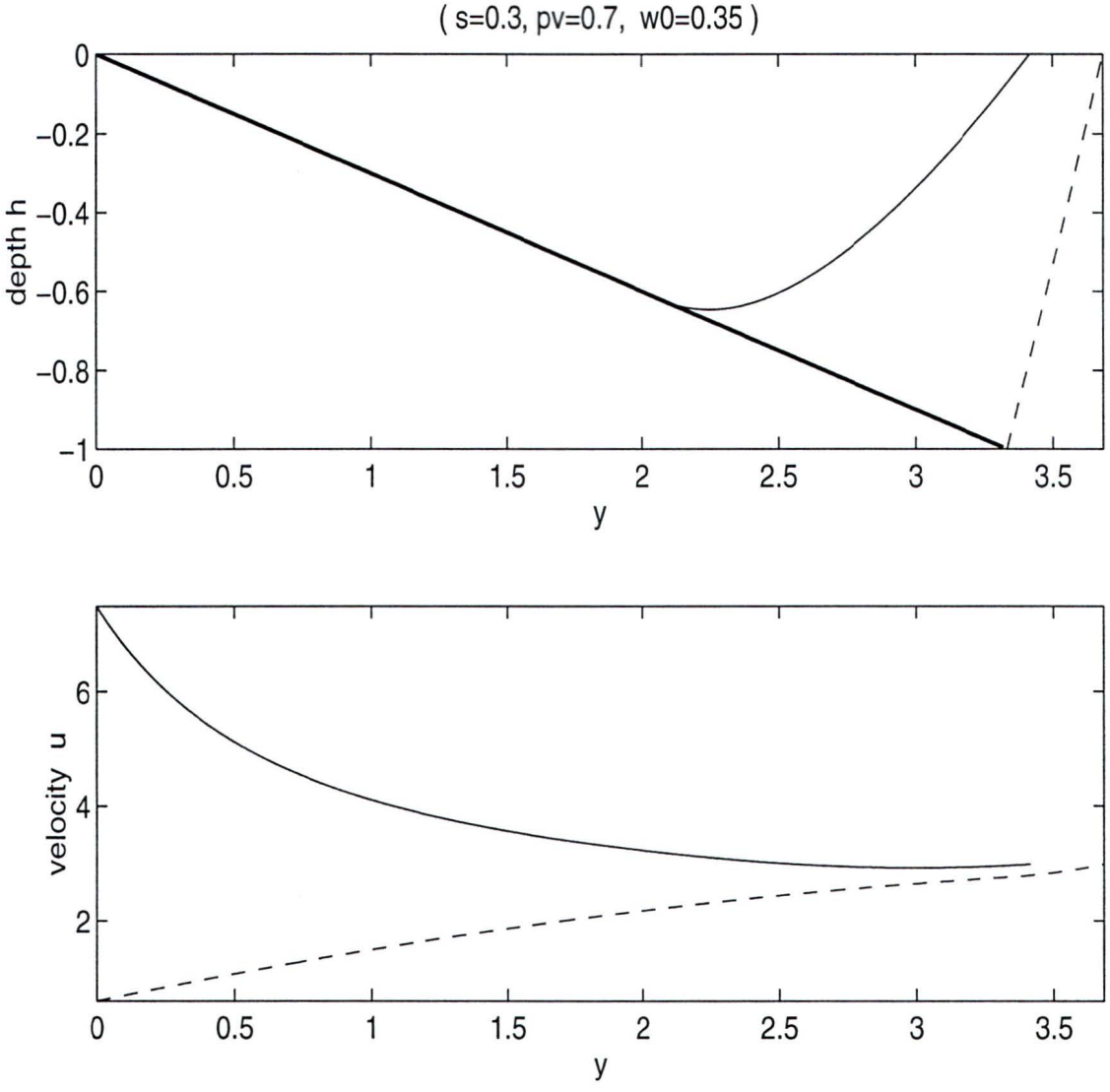

Figure 6.2: Simulation of the viscous case by choosing appropriate (s, δ, W_0) so that upstream (dashed lines) velocity at the wall is just above zero. The current speeds up greatly at the corner, indicating a large favourable pressure gradient upstream from the corner. The thick line in the depth profile indicates the sloping wall.

corner. Hence there must be an equally large *adverse* pressure gradient downstream where the coastline straightens out as opposed to the increase of curvature upstream. In that case, if friction is added, velocity around the corner will be greatly reduced, thus the chance for the flow to reverse downstream under the great adverse pressure gradient is great.

6.1.3 Effects of Three-Dimensionality

So far the model is only two-dimensional in the sense that velocity is considered constant with depth. In reality, especially in coastal waters, the water is shallow and bottom drag is important. Hence the velocity decreases near the bottom. What we have done so far can be considered as the depth average of a depth-dependent situation. Here we want to explore what effect the decrease of the velocity with depth has.

Generally, there are three forces in play: the pressure gradient, the Coriolis force and the centrifugal force. When averaged with depth, they are in balance. However, if the depth dependence is considered, that is, the velocity decreases with depth due to bottom drag, the balance breaks down. This is because the Coriolis force and the centrifugal force, being proportional to the velocity, change with depth, whereas the pressure gradient, according to the hydrostatic approximation, does not change with depth. It is shown in the following that this imbalance will cause cross-shore flow both at the upstream point and near the corner (Figure 6.3).

Upstream, with $\rho = \infty$, the forces in play are F_p, the pressure gradient offshore and F_c, the Coriolis force toward the shore. Averaged with depth, they are in balance. But as the bottom is approached and the velocity decreases, the Coriolis force decreases whereas the pressure gradient remains the same. As a result, there is a cross-stream current going away from the shore. Similarly, an inshore flow results

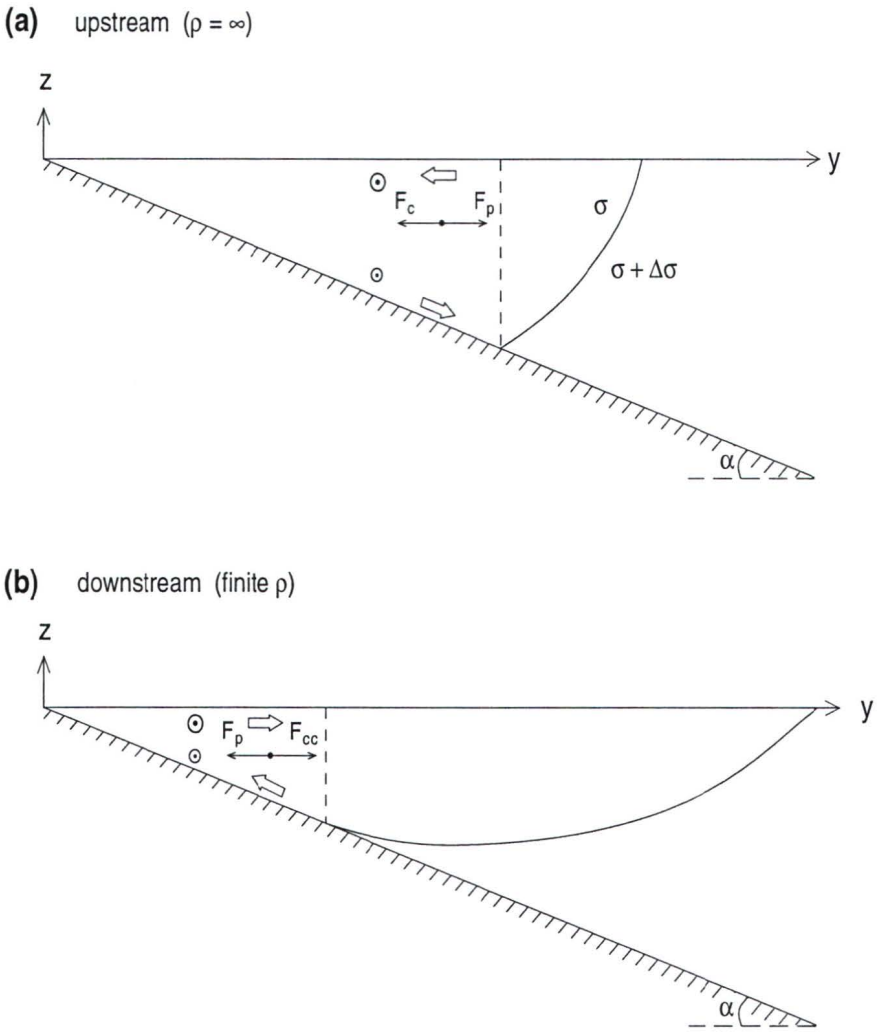

Figure 6.3: Schematic of the cross-sections with (a) $\rho = \infty$ and (b) finite ρ of a three-dimensional model with velocity decreasing with depth. Thin arrows represent the depth average of the forces: the pressure gradient $F_p = -p_y$, the Coriolis force $F_c = -u$, and $F_{cc} = u^2/(\rho + y) - u$, the sum of the centrifugal force and the Coriolis force. Thick arrows represent the transports at corresponding depths. The slope is $s = \tan\alpha$.

close to the surface. These two are in balance and there is no overall transport across the stream.

As one travels downstream, the curvature increases and the centrifugal force becomes important. The cross-stream momentum equation is

$$\frac{\mathrm{D}v}{\mathrm{D}t} = -u + \frac{u^2}{\rho + y} - \frac{\partial p}{\partial y}. \tag{6.6}$$

If we expand the depth-dependent variables according to

$$m(z) = \bar{m} + \varepsilon\, m'(z), \tag{6.7}$$

where, m can be either of the variables u, v, and ε is a small number, then (6.6) becomes

$$\frac{\mathrm{D}(\bar{v} + \varepsilon\, v'(z))}{\mathrm{D}t} = -\bar{u} - \varepsilon\, u'(z) + \frac{\bar{u}^2 + \varepsilon\, 2\bar{u}u'(z) + \varepsilon^2 u'(z)^2}{\rho + y} - \frac{\partial p}{\partial y}, \tag{6.8}$$

where $\partial p/\partial y$ is depth-independent.

To the lowest order, the forces are in balance and

$$\frac{\mathrm{D}\bar{v}}{\mathrm{D}t} = -\bar{u} + \frac{\bar{u}^2}{\rho + y} - \frac{\partial p}{\partial y} = 0. \tag{6.9}$$

To the first order, we have

$$\begin{aligned} \frac{\mathrm{D}v'(z)}{\mathrm{D}t} &= -u'(z) + \frac{2\bar{u}}{\rho + y} u'(z) \\ &= u'(z)\left(-1 + \frac{2\bar{u}}{\rho + y}\right), \end{aligned} \tag{6.10}$$

which indicates that $\bar{u} = (\rho + y)/2$ is the point where the cross-stream transport switches signs. Close to the bottom, $u'(z) < 0$. So when

$$\bar{u} > \frac{\rho + y}{2}, \tag{6.11}$$

the flow switches from offshore to inshore because $\mathrm{D}v'/\mathrm{D}t < 0$. This indicates that the transport becomes toward the shore even before the interface becomes flat ($\partial p/\partial y = 0$) at the intersection point, which requires $\bar{u} = \rho + y$ according to (6.9).

6.2 Applications

The surface current in the Barrow Canyon can be considered to have two layers, with the reduced gravity g' being about 0.02 ms^{-2}, and the upper layer thickness h_0 about 30 m (D'Asaro 1988). The latitude is about 70° N, giving $f \simeq 1.3 \times 10^{-4} s^{-1}$. Thus, the Rossby radius $R = \sqrt{g' h_0}/f$ is about 5.6 km. From Figure 6.4, the real slope s_0 near Point Barrow is about 0.9×10^{-2}, which corresponds to $s \simeq 1.7$ in our model according to $s = s_0/(h_0/R)$. Thus, from the model, $\rho_c \simeq u/f$. The 20 m isobath has a radius of curvature of about 20 km at Point Barrow (Figure 6.4), which requires a minimum velocity of 2.6 ms^{-1} for the current to separate. However, the maximum currents observed were 1.5 ms^{-1}, thus the interfacial upwelling mechanism cannot account for flow separation in this case. One possible mechanism is viscous boundary layer separation as suggested by D'Asaro (1988).

In the Strait of Gibraltar, where the current can also be considered to have two layers, the reduced gravity g' is about 0.02 ms^{-2}, the upper layer thickness is about 150 m. With $f \simeq 10^{-4} s^{-1}$, the Rossby radius R is about 17.3 km. The real slope s_0 is about 0.02 (Perkins et al. 1990), yielding $s \simeq 2.3$ in our model. Recall that the errors due to the simplification of the governing equations become considerable after $s > 2$, but here s is only slightly greater than 2, so if we were to apply the model result, the critical radius ρ_c would be about u/f. The 100 m isobath has a radius of curvature of 5 km (Figure 6.5), which requires $u > 0.5$ ms^{-1} for the current to separate. In practice, the surface flow has two possible basic states: the supercritical (at least 1 ms^{-1}) and the subcritical (can be less than 0.4 ms^{-1}). There can also be opposing barotropic flow (can be 0.5 Sverdrup) from Mediterranean to Atlantic. Thus supercritical flow will always lead to separation, whereas subcritical flow does not always separate (Bormans and Garrett 1989).

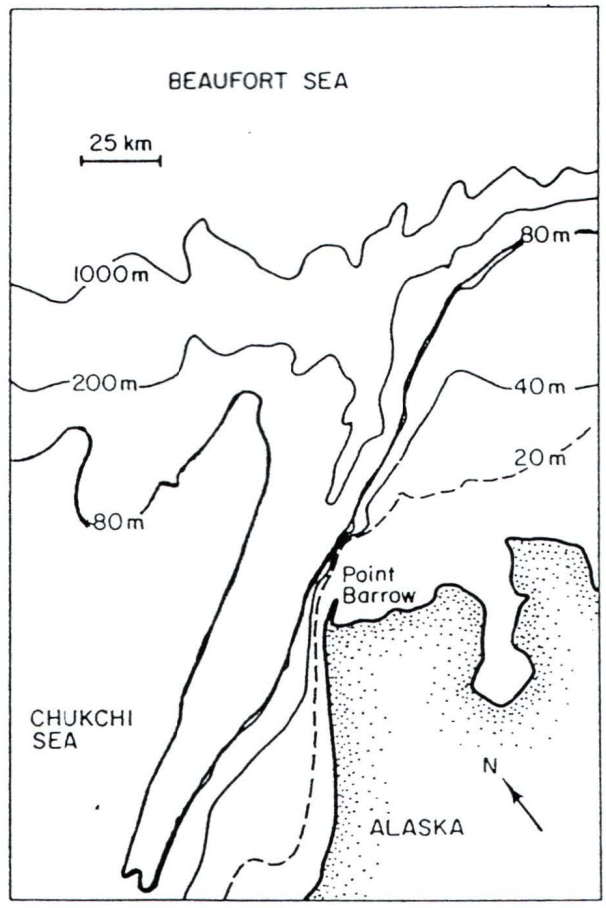

Figure 6.4: Topography of Barrow Canyon. Contours deeper than 1000 m are not shown. From Greenbern et al. (1979) and Garrison (1976).

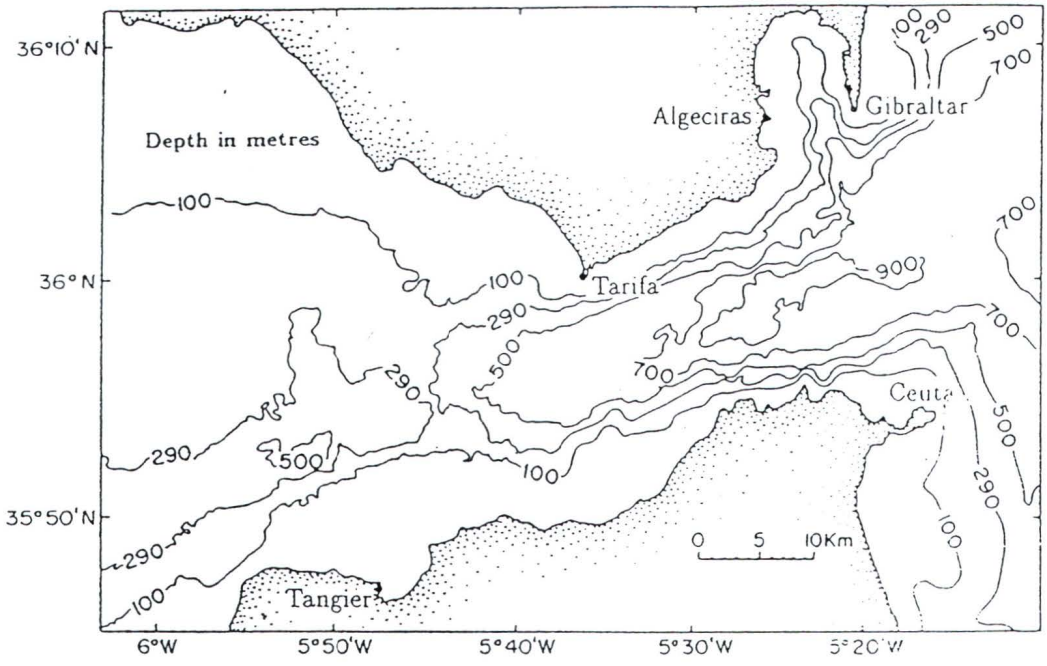

Figure 6.5: Bathymetry of the Strait of Gibraltar (Instituto Geografico Nacional y SECEG, 1988). Depth contours are in meters. The 290 m isobath has been chosen to show the location of the major sill to the west of Tarifa.

6.3 Conclusions

Coastline curvature can cause a stratified boundary current to separate from the coast through the mechanism of interfacial upwelling, that is, with the increase of coastline curvature, the centrifugal forces raise the density interface at the wall until it surfaces and separation occurs.

This mechanism has been studied using an inviscid, reduced gravity model in which the current is confined to the upper layer and insulated from the interior by a density front. The upstream potential vorticity is constant for simplicity. Klinger's (1994) work in which the coast has a vertical side is reproduced, and it agrees reasonably well with laboratory results that the critical radius of curvature ρ_c is approximately equal to the inertial radius of the current, $\overline{u}/f$.

A more realistic model in which the coast has a sloping side is developed, where the current is divided into a free region (where the slope effect is not felt) and a wedge region. With the upstream width of the free region and the upstream depth at the intersection point being kept equal to their vertical counterparts, cases with different slope s are compared in order to study the effect of the slope. The current is generally faster than its vertical counterpart, especially close to the wall. The critical radius of curvature ρ_c is almost identical to the vertical case for $s \geq 2$; for $s < 2$, ρ_c decreases with the decrease of s.

In both cases, it has been assumed that the alongshore variations have a larger length scale than the cross-shore ones, and hence the terms associated with cross-stream velocity and alongstream derivatives can be neglected. Whether this approximation is valid or not is checked at points just upstream of the separation points by comparing the neglected terms to the retained terms, using the depth and velocity fields obtained from the simplified governing equations.

In the vertical case, the ratios are generally $O(1)$, indicating that the approximation is not valid and it is recommended that the neglected terms be included in future studies. In the sloping case, the ratios decrease as s gets smaller. When $s < 2$, they are less than 0.5, thus the assumption can be considered valid.

The survey of parameter space undertaken confirms that, in both cases, no flow reversal occurs and upwelling of the interface is the only mode of separation available for this system.

This greatly simplified model gives some quantitative agreements with observed flows. Thus the hypothesis that, in a rotating system, centrifugal upwelling of a surface current's density interface can control the separation of the current from a curved coastline is strengthened.

Appendix A

Simplification of the Governing Equations

The governing equations are derived under the assumption that the alongshore variation length scale is long compared to the cross-shore one.

The original equations in dimensional form (following Røed 1980) are

$$\frac{u\,v_x}{1+y/\rho} + v\,v_y + fu - \frac{u^2}{\rho+y} = -g'h_y \tag{A.1}$$

$$f + \frac{v_x}{1+y/\rho} - u_y - \frac{u}{\rho+y} = h\delta, \tag{A.2}$$

where (x, y) are the coordinates parallel and perpendicular to the shore, respectively and (u, v) are the alongshore and cross-shore components of the velocity.

If the scales we use for non-dimensionalization are

$$D \text{ for } h, \quad \rho \text{ for } x, \quad W \text{ for } y,$$

$$U \text{ for } u, \quad V \text{ for } v,$$

then, according to the continuity equation

$$\frac{\partial}{\partial x}(hu) + \frac{\partial}{\partial y}\left(\frac{hv}{1+y/\rho}\right) = 0, \tag{A.3}$$

we have

$$\frac{U}{\rho} = \frac{V}{W}. \tag{A.4}$$

If we assume $W \ll \rho$, then a small number ε can be defined as

$$\varepsilon = W/\rho, \tag{A.5}$$

and from (A.4), we know

$$V = \varepsilon U. \tag{A.6}$$

Thus, the non-dimensional version of (A.1) and (A.2) is

$$\frac{U^2}{W}\left[\varepsilon^2\left(\frac{uv_x}{1+\varepsilon y} + vv_y\right) - \varepsilon\frac{u^2}{1+\varepsilon y}\right] + fUu = -\frac{g'D}{W}h_y \tag{A.7}$$

$$\frac{U}{W}\left[\varepsilon^2\frac{v_x}{1+\varepsilon y} - \varepsilon\left(u_y + \frac{u}{1+\varepsilon y}\right)\right] + f = Dh\delta. \tag{A.8}$$

Inside the square brackets on the left-hand side, the ε^2 terms can hence be neglected compared to the ε terms. In doing so, we have eliminated all the x derivatives, and are left with ordinary differential equations with respect to y only:

$$fu - \frac{u^2}{\rho + y} = -g'h_y \tag{A.9}$$

$$f - u_y - \frac{u}{\rho + y} = h\delta. \tag{A.10}$$

Bibliography

Ambar, I. & Howe, M., 1979a: Observations of the Mediterranean outflow. I. Mixing in the Mediterranean outflow. *Deep-Sea Research*, **26A**, 535–554.

Ambar, I. & Howe, M., 1979b: Observations of the Mediterranean outflow. II. The deep circulation in the vicinity of the Gulf of Cadiz. *Deep-Sea Research*, **26A**, 555–568.

Batchelor, G., 1967: *An Introduction to Fluid Dynamics.* Cambridge University Press.

Black, K.P., & Gay, S.L., 1987: Eddy formation in unsteady flows. *J. Geophys. Res.*, **92**, 9514–9522.

Bormans, M. & Garrett, C., 1989: A simple criterion for gyre formation by the surface outflow from a strait, with application to the Alboran Sea. *J. Geophys. Res.*, **94**, 12637–12644.

Bower, A., Armi, L. & Ambar, I., 1994: Direct evidence of meddy formation off the southwestern coast of Portugal. *Deep-Sea Research*, submitted.

Conlon, D. M., 1982:On the outflow modes of the Tsugaru Warm Current. *La Mer*, **20**, 60–64.

D'Asaro, E.A., 1988: Generation of submesoscale vortices: A new mechanism. *J. Geophys. Res.*, **93**, 6685–6693.

Donde Va Group, 1984: Donde Va? An oceanographic experiment in the Alboran Sea. *Eos, Transactions of the American Geophysical Union*, **65**, 682–683.

Garrison, G.R., Shaw, J.T. & Welch, M.L., 1982: Arctic oceanographic measurements: 1978-1980. *Rep. APL-UW 8112*, Appl. Phy. Lab., Univ. of Wash., Seattle.

Geyer, W.R. & Signell, R.P., 1990: Measurements of tidal flow around a headland with a shipboard acoustic Doppler current profiler. *J. Geophys. Res.*, **95**, 3189–3197.

Gill, A.E., 1982: *Atmosphere-Ocean Dynamics.* Academic Press.

Greenbern, J., Hart, P.E. & Grantz, A., 1979: Bathymetric chart of the continent shelf, slope and raise of the Beaufort Sea north of Alaska, *U.S. Geol. Surv. Open File Rep.*, **74–1313**, 6 pp..

Griffiths, R.W. & Linden, P.F., 1981: The stability of buoyancy-driven coastal currents. *Dyn. Atmos. Oceans*, **5**, 281-306.

Hufford, G.L., Thompson, B.D. & Farmer, L.D., 1977: Surface current of the northern Chuckchi Sea, Environmental Assessment of the Alaskan Continental Shelf. *Final Rep. RU-81*, 28 pp., Bur. of Land Manage., U.S. Dep. of the Inter..

Jones, S., 1977: Instabilities and wave interactions in a rotating two-layer fluid. PhD thesis, University of Cambridge.

Instituo Geografico Nacional y SECEG, 1988: Estrecho de Gibraltar, mapa fisico, Madrid.

Kawasaki, Y. & Sugimoto, T., 1984: Experimental studies on the formation and degeneration process of the Tsugaru warm gyre. In: *Ocean Hydrodynamics of the Japan and East China Sea*, Ichiye, T., editor, 225–238.

Klinger, B. A., 1992: Eddy generation at a convex corner by a coastal current in a rotating system. Ph.D. thesis, MIT-WHOI Joint Program in Oceanography.

Klinger, B. A., 1994: Inviscid current separation from rounded capes. *J. Phys. Oceanogr.*, **24**, 1805–1811.

Kundu, P.K., 1990: *Fluid Mechanics.* Academic Press.

Lanoix, F., 1974: Project Alboran. Etude hydrologique et dynamique de la Mer d'Alboran. *NATO Tech. Rep. 66*, Brussels.

Ou, H.W. & de Ruijter, W.P.M., 1986: Separation of an inertial current from a curved coastline. *J. Phys. Oceanogr.*, **16**, 280–289.

Pattiaratchi, C., James, A. & Collins, M., 1987: Island wakes and headland eddies: A comparison between remotely sensed data and laboratory experiments. *J. Geophys. Res.*, **92**, 783–794.

Perkins, H., Kinder, T.H. & LaViolette, P.E., 1990: The Atlantic inflow in the western Alboran Sea. *J. Phys. Oceanogr.*, **20**, 242–263.

Pingree, R., 1978: The formation of the Shambles and other banks by tidal stirring of the seas. *J. Mar. Biol. Assoc. U.K.*, **58**, 211–226.

Press, W.H., Flannery, B.P., Teukolsky, S.A. & Vetterling, W.T., 1986: *Numerical Recipes.* Cambridge University Press.

Røed, L.P., 1980: Curvature effects on hydraulically driven inertial boundary currents. *J. Fluid Mech.*, **96**, 395–412.

Schlichting, H., 1979: *Boundary Layer Theory.* 7th ed. McGrawHill.

Signell, R.P. & Geyer, W.R., 1991: Transient eddy formation around headlands. *J. Geophys. Res.*, **96**, 2561–2575.

Whitehead, J.A. & Miller, A.R., 1979: Laboratory simulation of the gyre in the Alboran Sea. *J. Geophys. Res.*, **84**, 3733–3742.

Wolanski, E., Imberger, J. & Heron, M., 1984: Island wakes in shallow coastal waters. *J. Geophys. Res.*, **89**, 10553–10569.

VITA

Surname: Jiang **Given Name: Xiaojun**

Place of Birth: Shandong, P.R.China Date of Birth: May 30, 1970

Educational Institutes Attended:

University of Victoria	1992 to 1995
Ocean University of Qingdao	1988 to 1992

Degrees Awarded:

B.Sc.	Ocean University of Qingdao	1992

Honours and Awards:

Graduate Teaching Fellowship	UVic	1991–94

PARTIAL COPYRIGHT LICENSE

Title of Thesis:

Flow Separation By Interfacial Upwelling In the Coastal Ocean

Author [redacted]

Xiaojun Jiang

September 12, 1995